Physical limits on kinesin-5–mediated chromosome congression in the smallest mitotic spindles

Kelsey M. McCoy[a,*], Emily S. Tubman[a], Allison Claas[a,†], Damien Tank[b], Shelly Applen Clancy[b], Eileen T. O'Toole[c,d], Judith Berman[b,e], and David J. Odde[a]

[a]Department of Biomedical Engineering and [b]Department of Genetics, Cell Biology, and Development, University of Minnesota, Minneapolis, MN 55455; [c]Molecular, Cellular, and Developmental Biology and [d]Boulder Laboratory for 3D Electron Microscopy of Cells, University of Colorado at Boulder, Boulder, CO 80309; [e]Department of Molecular Microbiology and Biotechnology, Tel Aviv University, Ramat Aviv 69978, Israel

ABSTRACT **A characteristic feature of mitotic spindles is the congression of chromosomes near the spindle equator, a process mediated by dynamic kinetochore microtubules. A major challenge is to understand how precise, submicrometer-scale control of kinetochore microtubule dynamics is achieved in the smallest mitotic spindles, where the noisiness of microtubule assembly/disassembly will potentially act to overwhelm the spatial information that controls microtubule plus end–tip positioning to mediate congression. To better understand this fundamental limit, we conducted an integrated live fluorescence, electron microscopy, and modeling analysis of the polymorphic fungal pathogen *Candida albicans*, which contains one of the smallest known mitotic spindles (<1 μm). Previously, ScCin8p (kinesin-5 in *Saccharomyces cerevisiae*) was shown to mediate chromosome congression by promoting catastrophe of long kinetochore microtubules (kMTs). Using *C. albicans* yeast and hyphal kinesin-5 (Kip1p) heterozygotes (*KIP1/kip1Δ*), we found that mutant spindles have longer kMTs than wild-type spindles, consistent with a less-organized spindle. By contrast, kinesin-8 heterozygous mutant (*KIP3/kip3Δ*) spindles exhibited the same spindle organization as wild type. Of interest, spindle organization in the yeast and hyphal states was indistinguishable, even though yeast and hyphal cell lengths differ by two- to fivefold, demonstrating that spindle length regulation and chromosome congression are intrinsic to the spindle and largely independent of cell size. Together these results are consistent with a kinesin-5–mediated, length-dependent depolymerase activity that organizes chromosomes at the spindle equator in *C. albicans* to overcome fundamental noisiness in microtubule self-assembly. More generally, we define a dimensionless number that sets a fundamental physical limit for maintaining congression in small spindles in the face of assembly noise and find that *C. albicans* operates very close to this limit, which may explain why it has the smallest known mitotic spindle that still manifests the classic congression architecture.**

Monitoring Editor
Alex Mogilner
University of California, Davis

Received: Oct 16, 2014
Revised: Aug 13, 2015
Accepted: Sep 3, 2015

This article was published online ahead of print in MBoC in Press (http://www.molbiolcell.org/cgi/doi/10.1091/mbc.E14-10-1454) on September 9, 2015.

Present addresses: *Department of Biological Sciences, Columbia University, New York, NY 10027; †Department of Biological Engineering, Massachusetts Institute of Technology, Cambridge, MA 02139.

Address correspondence to: David J. Odde (oddex002@umn.edu).

Abbreviations used: CV, coefficient of variation; iMT, interpolar microtubule; kMT, kinetochore microtubule; MT, microtubule; Pe, Peclet number; SNR, signal-to-noise ratio; SPB, spindle pole body.

INTRODUCTION

Mitosis, the phase of the cell cycle in which the replicated genome segregates to two daughter cells, requires the activity of dynamic microtubule plus ends that attach to chromosomes at kinetochores (Inoué and Salmon, 1995). Chromosome congression through the organization of dynamic kinetochore microtubules is widely observed and is necessary to establish an orderly preanaphase state. Several motor and kinetochore proteins are believed to drive congression, but the molecular mechanisms involved are not entirely clear (Inoué and Salmon, 1995; Gardner *et al.*, 2008; Gatlin and Bloom, 2010; Kops *et al.*, 2010; Westhorpe and Straight, 2013). The problem of spatial organization is especially acute in the smallest of eukaryotic spindles and raises the fundamental question of how spatial organization at the submicrometer scale is achieved in the face of stochastic microtubule length fluctuations.

One of the smallest mitotic spindles is that of the budding yeast *Saccharomyces cerevisiae*, which has metaphase spindle lengths of ~1.2–2.0 μm and kinetochore microtubule lengths of ~300–500 nm (Winey *et al.*, 1995; Yeh *et al.*, 1995; Maddox *et al.*, 2000; Gardner *et al.*, 2005, 2008; Shimogawa *et al.*, 2006; Tytell and Sorger, 2006). During mitosis in budding yeast, each kinetochore attaches to the plus end of a single kinetochore microtubule (kMT; Winey *et al.*, 1995; O'Toole *et al.*, 1999; Joglekar *et al.*, 2006, 2008). The kMTs grow in a length-dependent manner by which short MTs grow efficiently by net tubulin subunit addition and long MTs tend to undergo net shortening near the equator by removing tubulin subunits at their plus ends (Sprague *et al.*, 2003; Gardner *et al.*, 2005; Pearson *et al.*, 2006). The consequence of length-dependent growth is that kMT plus ends cluster in "attractor zones" located between the spindle pole bodies (SPBs) and spindle equator. Because the kinetochores are attached to the kMT plus ends, the chromosomes thus congress to the mitotic spindle equator. The result of the length-dependent growth appears as a characteristic bilobed distribution of fluorescent tubulin in budding yeast, in which the loss of fluorescence near the spindle equator indicates the absence of tubulin and demonstrates that the kMT plus ends cluster at attractor zones located on opposite sides of the equator, typically near the quarter-spindle position (Maddox *et al.*, 2000; Sprague *et al.*, 2003; Gardner *et al.*, 2005, 2008).

A study of budding yeast by Gardner *et al.* (2008) found that deletion of Cin8p, the major kinesin-5 motor protein in *S. cerevisiae,* and to a lesser extent the minor kinesin-5 Kip1p led to a phenotype that lacked the bilobed tubulin fluorescence distribution characteristic of wild-type metaphase spindles, indicating that the kMTs of the *cin8Δ* spindles were both longer and more variable in length than in the wild-type cells and suggesting that the chromosome alignment was subsequently disrupted. They also found that a *cin8Δ* mutant lacking the nuclear localization sequence also lacked spindle organization and that *cin8* mutants had longer astral MTs (aMTs) than the wild-type parental strain. Through this work and many other experiments, including electron microscopy to visualize the individual spindle MTs, fluorescence recovery after photobleaching of kinetochores and spindle MTs to determine where tubulin turnover is fastest, and fluorescent visualization of the Cin8p motors to determine their dynamics and distribution on the spindles, Gardner *et al.* (2008) discovered that Cin8p is responsible for the length-dependent growth pattern of kMTs found experimentally in budding yeast. A model that explains these experimental observations proposes that kinesin-5 motors act as length-dependent MT depolymerases, promoting catastrophe (the switch from a growing, polymerizing state to a shortening, depolymerizing state) of long MTs (Gardner *et al.*, 2008). In this model, kinesin-5 motors walk toward MT plus ends and, upon arrival, promote catastrophe. Because long MTs have more binding sites for kinesin-5 motors, they are more likely to accumulate motors at their plus ends and undergo catastrophe. Short MTs, however, provide fewer binding sites, making catastrophe less frequent and allowing the MTs to grow more efficiently. Because of its preferential accumulation at the growing tips of longer kMTs compared with shorter kMTs, kinesin-5 in budding yeast is a *length-dependent* depolymerase that provides a self-organizing mechanism to congress chromosomes even in the 1- to 2-μm budding yeast spindle.

The role as a length-dependent depolymerase adds to the known role of kinesin-5 in cross-linking antiparallel interpolar MTs and walking toward their plus ends to generate a force that slides them apart, thereby elongating and stabilizing the bipolar spindle (Enos and Morris, 1990; Hagan and Yanagida, 1990; Cole *et al.*, 1994; Kashlna *et al.*, 1996; Hildebrandt and Hoyt, 2000; Kapitein *et al.*, 2005). In addition, this new role is similar to the length-dependent depolymerase activity of the motor protein kinesin-8 in yeast in vitro (Gupta *et al.*, 2006; Varga *et al.*, 2006; Stumpff *et al.*, 2007). However, Gardner *et al.* (2008) found that kinesin-8 motors (Kip3p in *S. cerevisiae*) have no detectable effect on kMT length regulation in vivo; instead, kinesin-8 acts primarily on interpolar microtubules (iMTs), implying that kinesin-5 is primarily responsible for kMT length regulation in budding yeast. This differential effect of kinesin motors on the different types of spindle MTs is explained by the homotetrameric structure of kinesin-5, which preferentially binds in areas of high polymer density, where both motor heads can bind simultaneously. Accordingly, the lower polymer density of iMTs limits the ability of kinesin-5 to gain access to iMT plus ends. In contrast, the homodimeric structure of kinesin-8 can only bind to a single MT at a time, allowing it relatively unimpeded access to the plus ends of long iMTs (Gardner *et al.*, 2008).

Although the length-dependent depolymerase activity of kinesin-5 was detected in *S. cerevisiae*, it is not known whether this mechanism is generalizable to other organisms, particularly ones whose steady-state metaphase spindles are even shorter than in budding yeast—for example, <1 μm. As spindles become shorter, their kinetochore microtubules, typically 35–45% of spindle length, must also become proportionately shorter, making the requirements for achieving congression even more demanding. In the limit, the length scales of the kMTs will start to approach the nanoscale of the tubulin dimers themselves (8 nm), so that stochastic growth and shortening dynamics, known as directional instability (Inoue and Salmon, 1995), will create sufficient "noise" to overwhelm the positioning signal located at the attractor zone as determined by the motor-mediated catastrophe gradient. As illustrated in Figure 1, the precision of congression can be quantified as the SD of kMT lengths, σ, which can in turn be normalized to the mean kMT length, $\langle L \rangle$, to define the coefficient of variation, $CV = \sigma/\langle L \rangle$. In engineering terms, noise in signals is often quantified as the signal-to-noise ratio, SNR, and in this case, $SNR = \langle L \rangle/\sigma = 1/CV$. In the case of no length control at all, the length distribution of microtubules will be exponential (Hill and Chen, 1984), in which case the mean equals the SD ($\langle L \rangle = \sigma$), and so $CV = SNR = 1$. So, a fundamental question in biology is, what sets the lower physical limit on absolute size of congressed mitotic spindles?

To address this question, we used the methods developed by Gardner *et al.* (2008) to study chromosome congression in the pathogenic yeast *Candida albicans*, which has one of the smallest known eukaryotic mitotic spindles at ~0.8 μm. *C. albicans* is a diploid yeast that has three distinct morphologies—budding yeast, pseudohyphae, and hyphae—with the multicellular hyphal morphology believed to be important for virulence (Berman, 2006; Brand, 2012).

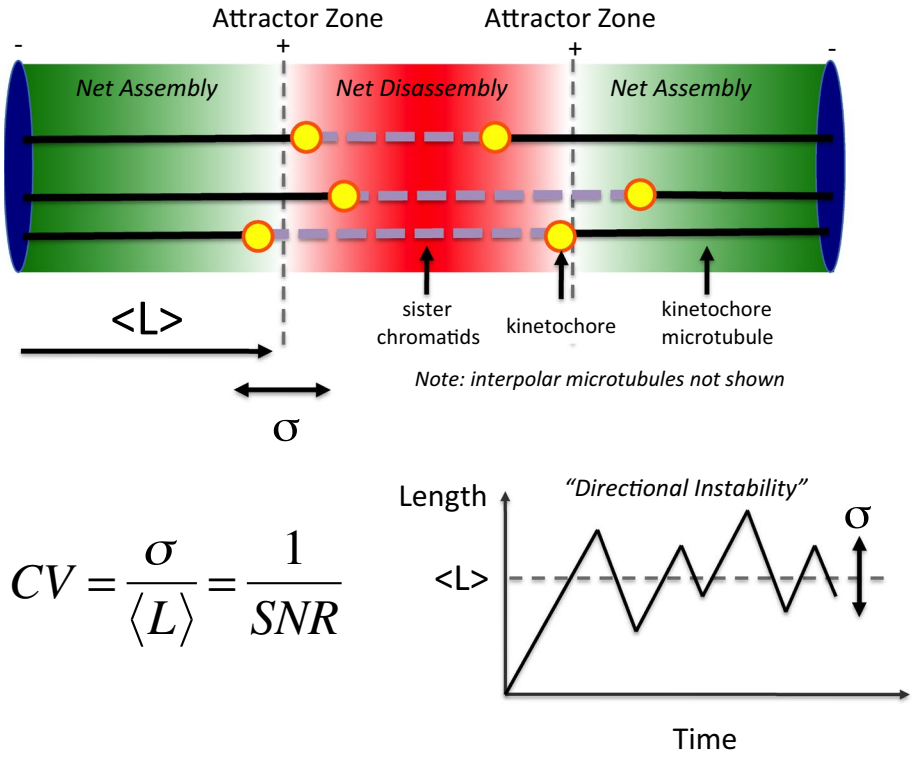

FIGURE 1: Noise in chromosome congression. Schematic of kMT organization illustrating that kMTs need to have a relatively small SD of length (σ) relative to mean length (<*L*>) if they are to manifest a congressed state. The level of noise in chromosome congression can be quantified by the CV, which is the ratio of σ to <*L*>. Another common measure of noise in a signal is the SNR, which is the inverse of the CV. The level of noise in assembly physically originates from directional instability, the stochastic transitions between net kMT assembly (away from poleward movement), and net kMT disassembly (poleward movement) due to net αβ-tubulin subunit addition/loss as kMTs undergo dynamic instability.

C. albicans yeast cells morphologically resemble budding yeast cells (Finley and Berman, 2005; Table 1). In addition, *C. albicans* can be induced to form hyphae, which are much longer and narrower than yeast cells. In hyphae, before mitosis, nuclei migrate much larger distances than they do in yeast cells, and anaphase spindle lengths are also much longer in hyphae than in yeast cells (Finley and Berman, 2005). Thus *C. albicans* yeast cells are ideal for testing predictions of the kinesin-5–mediated, self-organized model of chromosome congression in a different organism, and *C. albicans* hyphal cells provide the opportunity to determine the effect of cell dimensions on mitotic spindle properties. Although some green algae and trypanosomes also have small spindles (0.5–1.0 μm), they lack sufficient numbers of microtubules to achieve a minimal 1:1 coupling of microtubules to chromosomes and thus likely operate by an alternative mechanism relative to the more classic model for mitosis (Gan *et al.*, 2011). Thus *C. albicans* is an excellent model organism with which to explore classic mitosis at very small length scales.

RESULTS

A dimensionless number that sets theoretical lower physical limits on congression

To establish the lower limits on mitotic spindle congression, we developed a mathematical theory that predicts the CV, or equivalently the SNR (Figure 1), based on the assembly-disassembly dynamics of kMTs (see the Supplemental Material). For small CV (large SNR), a spindle will exhibit strict length control to achieve a well-organized congressed state while simultaneously remaining dynamic and exhibiting directional instability. For animal spindles, we estimate values roughly ranging from <*L*> ≈ 8.3 μm and σ ≈ 1.35 μm for CV = 0.16 in a *Potorous tridactylus* PtK1 cell (Cimini *et al.*, 2004) to <*L*> ≈ 3.1 μm and σ ≈ 0.56 μm for CV = 0.18 in a *Drosophila melanogaster* S2 cell (see the Supplemental Material). Therefore it appears that CV ≈ 0.15–0.20 (SNR = 5–6) is characteristic of a well-organized, congressed state in an animal mitotic spindle. We wondered whether very small spindles, such as those in *C. albicans*, would theoretically be able to achieve congression, and so we developed a mathematical model to predict the lower physical limits on congression, that is, when CV = 1.

Our mathematical model, based on Figure 1 and detailed in the Supplemental Material, gives the CV in terms of a dimensionless Peclet number, Pe, given by

$$\mathrm{Pe} = \frac{V\langle L \rangle}{D} \qquad (1)$$

where Pe characterizes the relative strength of convective transport (*V*, the rate at which microtubules grow and shorten, i.e., the velocity of directional instability) relative to diffusive transport (*D*, the rate at which random switching between growth and shortening states acts to randomize the tip position), scaled by the size of the system (<*L*>, the mean length of microtubules). The Peclet number is commonly used to assess whether convection or diffusion is the dominant transport mechanism. In physical terms, a large Pe means that there is a very strong tendency for a kMT plus end to "drift" toward the attractor, whereas a low Pe means that kMT plus-end "diffusion" due to stochastic dynamic instability switching is dominant, disrupting the ability of the kMT plus end to be positioned near the attractor. As shown in the Supplemental Material, the CV is related to the Peclet number by

	S. cerevisiae	*C. albicans*
Ploidy	Haploid (O'Toole *et al.*, 1999)	Diploid (Joglekar *et al.*, 2008)
Kinesin-5 motor proteins	Cin8p, Kip1p (Hildebrandt and Hoyt, 2000)	Kip1p (Chua *et al.*, 2007)
Number of chromosomes	16 haploid (O'Toole *et al.* 1999; Winey and O'Toole, 2001)	8 diploid (16 total; Joglekar *et al.*, 2008)
Number of kMTs/kinetochore	1 (O'Toole *et al.* 1999; Winey and O'Toole, 2001)	1 (Joglekar *et al.*, 2008; Burrack *et al.*, 2011)

TABLE 1: Selected comparison between *S. cerevisiae* and *C. albicans*.

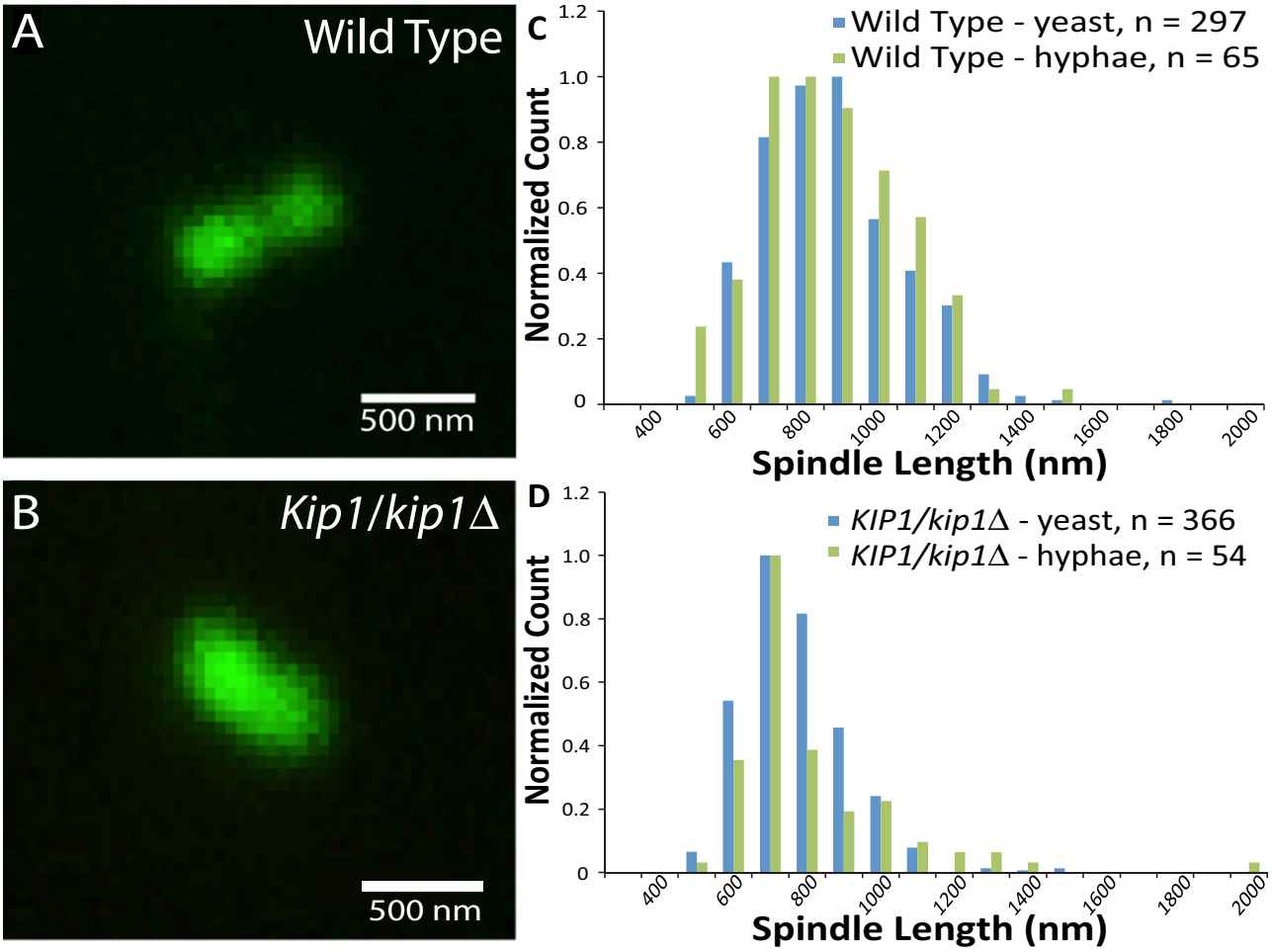

FIGURE 2: Spindle lengths in *C. albicans*. Cells in the hyphal morphology have spindle lengths similar to cells in the budding yeast morphology. (A) Example experimental image of Tub1-GFP fluorescence in a yeast WT spindle (strain used was YJB12377). (B) Example experimental image of Tub1-GFP fluorescence in a yeast *KIP1/kip1Δ* spindle (stain used was YJB12711). (C) Histogram of WT Tub1-GFP spindle lengths for the yeast and hyphal morphologies, showing the same length distribution regardless of cell morphology (strain used was YJB12377). (D) Histogram of the *KIP1/kip1Δ* Tub1-GFP spindle lengths for the yeast and hyphal morphologies, showing the same distribution regardless of morphology. Spindles in both cases are shorter than WT spindles (strain used was YJB12711).

$$\frac{\sigma}{\langle L \rangle} = \sqrt{\frac{2}{\mathrm{Pe}}} \tag{2}$$

In terms of microtubule assembly parameters, we can rewrite Eq. 2 as

$$\frac{\sigma}{\langle L \rangle} = \sqrt{V\beta\tau} \tag{3}$$

where V is the velocity of directional instability ($V \approx V_g \approx V_s$, where V_g and V_s are the kMT growth and shortening rates, respectively), β is the strength of the catastrophe gradient (indicated by the green to red shading with increasing kMT length in Figure 1), and τ is the mean time for switching between growth and shortening states ($\tau \approx 1/k_c(\langle L \rangle) \approx 1/k_r(\langle L \rangle)$, where $k_c(\langle L \rangle)$ and $k_r(\langle L \rangle)$ are the catastrophe and rescue frequencies when a kMT has length $\langle L \rangle$, respectively). A detailed derivation is provided in the Supplemental Material. In the present study, we consider that the gradient is mediated by molecular motors as previously described (Gardner *et al.*, 2008), although the analysis does not specifically require this assumption, and the gradient could principle be in mediated via a phosphostate gradient, for example (Sprague *et al.*, 2003)

Using previous estimates for *S. cerevisiae* (Gardner *et al.*, 2008; see Supplemental Table S3), we estimate $V = 1.2$ μm/min, $\beta = 28$ μm^{-1} min^{-1}, $\langle L \rangle = 0.49$ μm, and $k_c(\langle L \rangle) = k_r(\langle L \rangle) = 14$ min^{-1}, and therefore $\tau = 0.053$ min, which yields Pe = 11 or, equivalently, CV = 0.43, in reasonable agreement with the direct experimental observations cited. For Cin8Δ in *S. cerevisiae*, we estimate $V = 1.9$ μm/min, $\beta = 17$ μm^{-1} min^{-1}, $\langle L \rangle = 0.56$ μm, $k_c(\langle L \rangle) = k_r(\langle L \rangle) = 9.7$ min^{-1}, and therefore $\tau = 0.10$ min, which yields Pe = 5.8 or, equivalently, CV = 0.59, consistent with a more poorly congressed spindle. Because the *C. albicans* spindle is even shorter than the S. cerevisiae spindle, the theory predicts that *C. albicans* is near the limits. To address this question and estimate CV for *C. albicans*, we conducted a quantitative analysis of the *C. albicans* spindle length and congression in wild-type and reduced kinesin-5/kinesin-8 motor levels.

KIP1/kip1Δ spindles are shorter on average than wild-type spindles

To characterize quantitatively the mitotic spindle of *C. albicans*, we measured the metaphase spindle length as defined by the distance from minus end to minus end using green fluorescent protein (GFP)–tagged α-tubulin (Figure 2) in both yeast and hyphal cells. Of

interest, we measured the yeast mitotic spindle length to be 842 ± 6 nm (±SEM; $n = 297$), which is approximately twofold to threefold shorter than that for other fungal species, such as *S. cerevisiae* and *Schizosaccharomyces pombe* (Goshima *et al.*, 1999; Gardner *et al.*, 2008).

Given the spindle-elongating sliding activity of kinesin-5 in other species, reducing the amount of Kip1p on the spindle is expected to decrease the outward force on the SPBs, thus decreasing the spindle length. Consistent with this expectation, the mean length of the *KIP1/kip1Δ* metaphase spindles was 766 ± 8 nm (±SEM; $n = 366$), which is statistically shorter than the wild-type (WT) spindle length of 842 ± 6 nm (±SEM; $n = 297$; $p < 0.0001$; Student's *t* test). These results indicate that the reduction in the number of Kip1p motors decreases the observed effects of the motors, as predicted, demonstrating that the spindle length is sensitive to the total number of motors present.

Hyphal and yeast mitotic spindle length and shape are similar

Of interest, hyphal metaphase spindles as measured from SPB to SPB followed the same pattern, with the mean *KIP1/kip1Δ* spindle length of 760 ± 19 nm (±SEM; $n = 54$) being significantly shorter than the WT spindle length of 854 ± 19 nm (±SEM; $n = 65$; $p = 8.87 \times 10^{-4}$; Student's *t* test). Of importance, mean hyphal spindle lengths were not statistically different from the corresponding budding yeast spindles, with $p = 0.54$ for the WT spindles and 0.75 for the *KIP1/kip1Δ* spindles (Student's *t* test). The hyphal spindles also had the same spindle length distributions as the yeast spindles (Figure 2, C and D), confirming that the spindle length as measured from SPB to SPB is independent of cell morphology/morphogenetic stage. This result, combined with similar distribution patterns of Tub1-GFP fluorescence (Figure 3, A, B, and E), demonstrates that there is no significant difference between the metaphase spindles of the budding yeast and hyphal cell morphologies, despite the hyphal cells being twofold to fivefold longer than yeast cells. We conclude that Kip1p effects on spindle shape and spindle length are robust with respect to local cell shape and size. In light of this result, all other experiments were performed using only cells with the budding yeast morphology.

Tubulin-GFP fluorescence distribution is consistent with longer kMTs in KIP1/kip1Δ cells than in wild-type cells

If kinesin-5 (Kip1p in *C. albicans*; Chua *et al.*, 2007) promotes kMT disassembly by a length-dependent mechanism (Gardner *et al.*, 2008), then the kMTs in the *KIP1/kip1Δ* spindles should be longer than the WT kMTs. Quantitative analysis of metaphase WT spindles revealed the characteristic bilobed distribution of tubulin fluorescence, with a decrease in fluorescence intensity near the spindle equator, indicating reduced amounts of microtubule density at the equator (Figure 3, A and B). This suggests that, as in *S. cerevisiae*, kMT plus ends generally terminate before reaching the equator in *C. albicans*. To measure this effect, we analyzed metaphase spindles.

Metaphase was defined using a length criterion by which all spindles within 1 SD of the average spindle length (842 ± 6 nm, $n = 297$, error reported as SEM) were considered to be in metaphase (Gardner *et al.*, 2008; Supplemental Figure S1). Mutant spindles were analyzed using the wild-type length criterion to control for length-dependent effects. Quantitative analysis of the *KIP1/kip1Δ* spindles showed a statistically significant shift in fluorescence toward the spindle equator, indicating that the kMTs extend through the spindle equator, where they contribute fluorescence

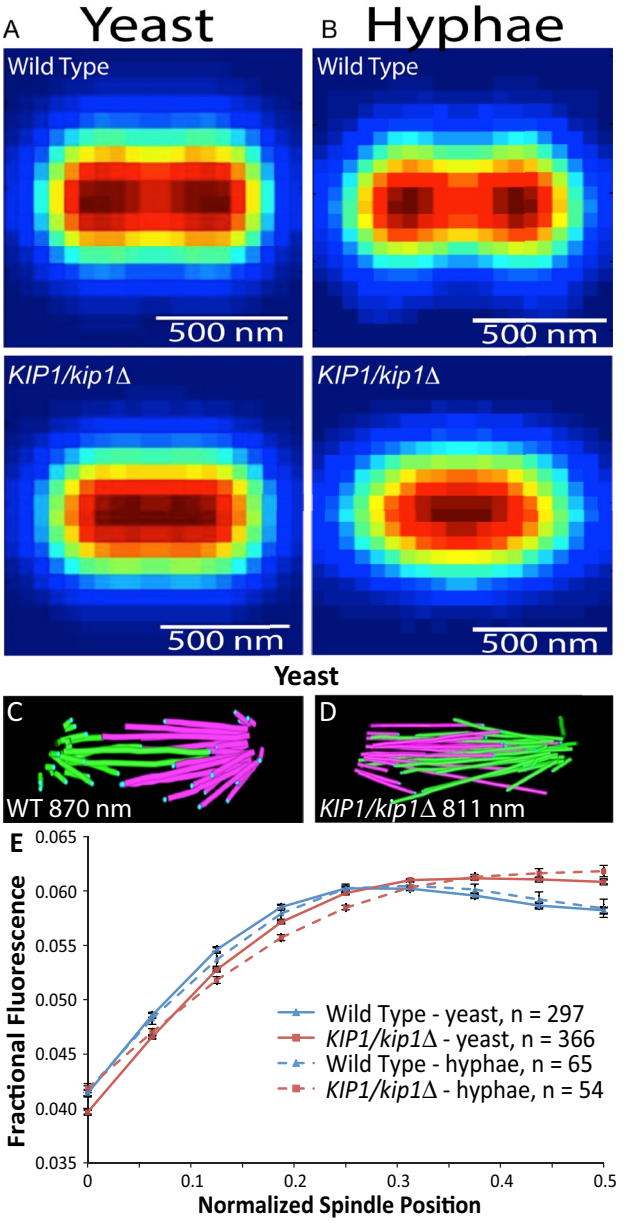

FIGURE 3: Kip1p deletion results in longer kMTs in *C. albicans*. (A) Heat map composite of Tub1-GFP fluorescence intensity for yeast WT and *KIP1/kip1Δ* spindles. The WT spindles exhibit the characteristic bilobed fluorescence distribution, and the *KIP1/kip1Δ* spindles have no such bilobed distribution, appearing instead as a single bar of fluorescence (30 and 36 cells; strains used were YJB12377 and YJB12711). (B) Heat map composite of Tub1-GFP fluorescence intensity of hyphae WT and *KIP1/kip1Δ* metaphase spindle. The WT spindles exhibit the characteristic bilobed fluorescence distribution, and the *KIP1/kip1Δ* spindles have no such bilobed distribution, appearing instead as a single bar of fluorescence (35 and 33 cells; strains used were YJB12711 and YJB12377). (C) ET reconstruction tomogram of a WT yeast spindle (strain used was YJB12377). (D) ET reconstruction tomogram of a *KIP1/kip1Δ* yeast spindle (strain used was YJB12711). (E) Normalized fluorescence distribution for Tub1-GFP of the yeast and hyphal morphologies. The WT spindles display a decrease in fluorescence near the spindle equator that does not appear in the *KIP1/kip1Δ* spindles, demonstrating that the *KIP1/kip1Δ* spindles have longer and more varied kMTs on average than the WT spindles (strains used were YJB12377 and YJB12711).

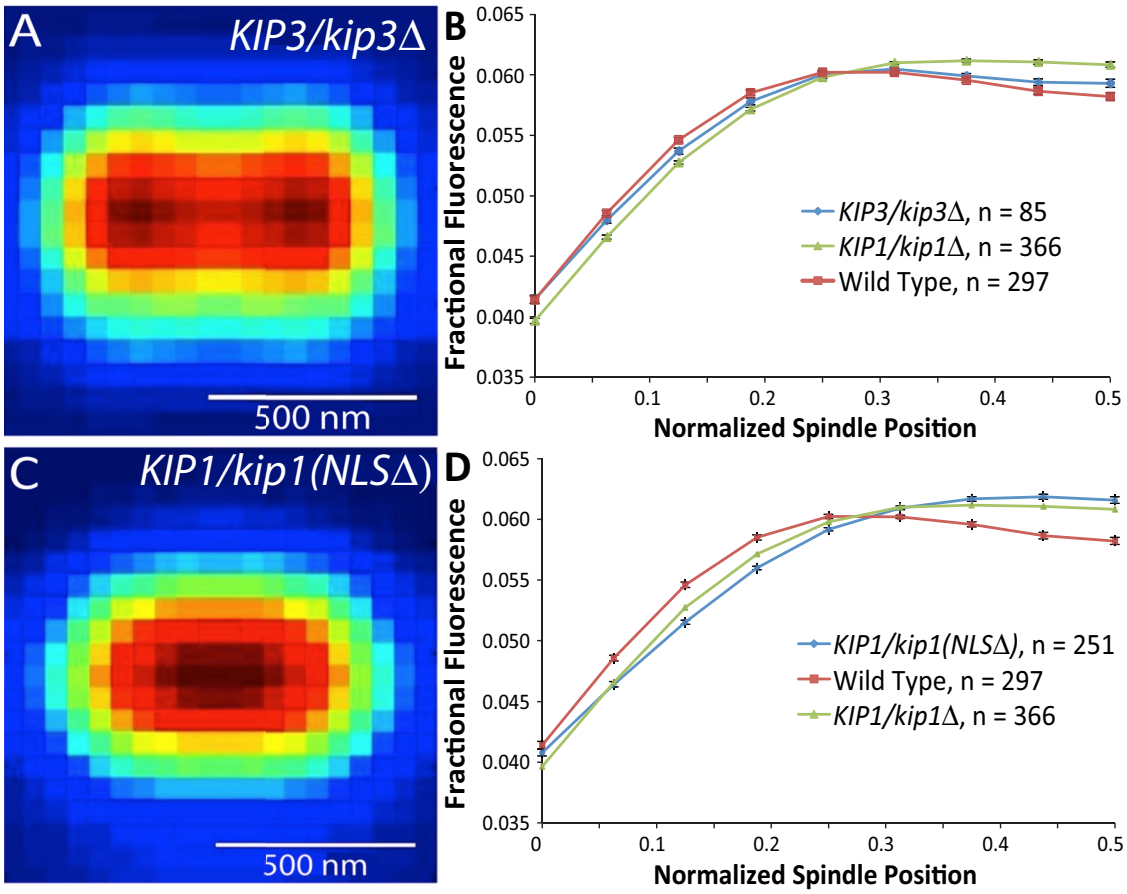

FIGURE 4: Kip3p deletion does not result in longer kMTs in *C. albicans* yeast, but deletion of the Kip1p NLS results in longer kMTs. (A) Heat map composite of Tub1-GFP fluorescence intensity for *KIP3/kip3Δ* spindles, which exhibited the bilobed fluorescence distribution characteristic of the WT spindles (30 cells; strain used was YJB13121). (B) Normalized fluorescence distribution for Tub1-GFP of the budding yeast morphology for *KIP3/kip3Δ*, WT, and *KIP1/kip1Δ*. The *KIP3/kip3Δ* is statistically the same as the WT distribution ($p = 0.12$) and statistically different from the *KIP1/kip1Δ* distribution ($p < 0.0001$; strains used were YJB12377, YJB12711, and YJB13121 respectively). (C) Heat map composite of fluorescence intensity for *KIP1/kip1(NLSΔ)* spindles, which exhibit the same Tub1-GFP fluorescence intensity distribution as *KIP1/kip1Δ* (strain used was YJB13143). (D) Normalized fluorescence intensity distribution for Tub1-GFP for *KIP1/kip1(NLSΔ)*, WT, and *KIP1/kip1Δ* spindles. The *KIP1/kip1(NLSΔ)* spindles have a similar distribution to the *KIP1/kip1Δ* spindles ($p = 0.0002$) and do not exhibit any significant decrease in fluorescence near the spindle equator (strains used were YJB12377, YJB12711, and YJB13143).

signal, and their plus ends terminate at or past the equator (Figure 3, A and B; $p < 0.0001$; bootstrap statistical method described in the Supplemental Material used unless otherwise noted). Electron tomography (ET) reconstruction of a *KIP1/kip1Δ* spindle confirmed that MTs in the mutant are longer than in the WT and that the mutant spindle is less organized overall (Figure 3, C and D). Together the fluorescence and electron microscopy measurements confirmed the prediction that, as in *S. cerevisiae*, *C. albicans* cells with reduced levels of kinesin-5 have longer kMTs and fail to properly organize spindle microtubules. Of interest, despite very different cell sizes, metaphase spindles of cells with the budding yeast morphology and the hyphal morphology yielded very similar results: *KIP1/kip1Δ* kMTs were longer and more disorganized than WT spindles (Figure 3E).

KIP3/kip3Δ kMTs display similar organization to WT kMTs

The self-organized assembly model (Gardner *et al.*, 2008) predicts that kinesin-8 (encoded by *KIP3* in *C. albicans*) primarily regulates the length of iMTs, and thus *KIP3/kip3Δ* heterozygotes should have well-congressed spindles compared with the spindles in *KIP1/kip1Δ* heterozygotes. Indeed, the Tub1-GFP fluorescence in *KIP3/kip3Δ* spindles showed the same distribution as WT, with a characteristic decrease near the spindle equator, suggesting that kMT lengths in the *KIP3/kip3Δ* spindles are, on average, the same as WT (Figure 4B, $n = 86$, $p = 0.12$). This trend differs from that for the *KIP1/kip1Δ* spindles, which lack the decrease in fluorescence near the spindle equator (Figure 2, C and D), suggesting that the kMT lengths in the *KIP3/kip3Δ* spindles are on average shorter than in the *KIP1/kip1Δ* ($p < 0.0001$) spindles (Figure 4B). Nonetheless, the *KIP3/kip3Δ* spindle lengths (961 ± 9 nm; *KIP3/kip3Δ* ± SEM; $n = 86$) were longer than the WT spindle lengths (842 ± 6 nm; WT ± SEM; $n = 297$; $p < 0.0001$; Student's *t* test), consistent with the proposed iMT depolymerase activity of Kip3p, which preferentially regulates iMT length (Gardner *et al.*, 2008). Our observation that the *KIP3/kip3Δ* spindles exhibit the same level of kMT organization as WT, in that the spindles display a decrease in Tub1-GFP fluorescence at the spindle equator, suggests that Kip3p is not responsible for kMT length regulation during metaphase in *C. albicans*.

KIP1/kip1(NLSΔ) spindles phenocopy KIP1/kip1Δ Tub1-GFP distribution

The length-dependent disassembly model for kinesin-5 predicts that the net depolymerase effect of Kip1p is directly dependent on the number of motors on the spindle itself rather than indirectly through the total number of motors in the cell. Therefore deleting the nuclear localization sequence (NLS) of one copy of Kip1p, which presumably would restrict half of the available Kip1p from entering the nucleus, is predicted to result in longer, less-organized kMTs, similar to those seen in the *KIP1/kip1Δ* heterozygous mutant. Consistent with this prediction and with experimental results for the analogous kinesin-5 NLS deletion mutants in *S. cerevisiae* (Gardner *et al.*, 2008), spindles in *C. albicans KIP1/kip1(NLSΔ)* cells exhibited a Tub1-GFP fluorescence intensity distribution similar to that of spindles in the *KIP1/kip1Δ* cells: the relative fluorescence intensity near the spindle equator was higher than in the WT cells ($p = 0.0002$; Figure 4, C and D). In addition, the *KIP1/kip1(NLSΔ)* spindles also were observed to be shorter than WT spindles (812 ± 8 nm; *KIP1/kip1(NLSΔ)* ± SEM; $p = 0.008$; Student's *t* test) but longer than *KIP1/kip1Δ* spindles ($p < 1 \times 10^{-4}$; Student's *t* test). This is likely due to the partitioning of half of the Kip1p motors outside of the nucleus during mitosis, because *C. albicans,* like *S. cerevisiae*, undergoes a closed mitosis in which the nuclear envelope does not break down (Berman, 2006). Because some of the motors cannot access the spindle during mitosis, they cannot affect spindle organization. This result confirms that it is the number of motors in the nucleus, and thus on the mitotic spindle, that affects kMT length and organization rather than the global number of motors present in the cell.

Astral MT length depends on concentration of motors in the cytosol

Deleting the NLS presumably increases the concentration of motors outside of the nucleus and, thus, according to the length-dependent disassembly model of kinesin-5, should decrease the average aMT length as a function of the concentration of motors outside of the nucleus. Consistent with this, the aMTs of the *KIP1/kip1(NLSΔ)* spindles were shorter (850 ± 70 nm [±SEM]; $n = 87$) than the WT aMTs ($p = 9 \times 10^{-5}$; Student's *t* test; Figure 5). By this same logic, reducing the overall number of motors should also increase the aMT length. This effect was seen in the aMTs in the cytosol of the *KIP1/kip1Δ* cells, which were longer (1800 ± 130 nm [±SEM]; $n = 44$) than the WT aMTs (1300 ± 90 nm [±SEM]; $n = 54$; $p = 0.001$; Student's *t* test; Figure 5A).

The role of kinesin-8 in aMT length is to depolymerize aMTs, and, thus, reducing the total amount of Kip3p by 50% in *KIP3/kip3Δ* strains is expected to reduce the number of depolymerases and increase aMT length (Gupta *et al.*, 2006; Varga *et al.*, 2006). Consistent with this prediction, the aMTs of *KIP3/kip3Δ* spindles were longer (2400 ± 120 nm [±SEM]; $n = 79$) than WT aMTs ($p = 6 \times 10^{-10}$; Student's *t* test), as expected based on the Kip3p depolymerase activity. This significant increase in the aMT length compared with the *KIP1/kip1Δ* cells is consistent with the model's prediction that the Kip3p dimers are more likely to bind to MTs without nearby MTs to cross-link, such as aMTs, than the Kip1p tetramers, which preferentially bind to kMTs due to the increased cross-linking potential.

Taken together, these results demonstrate that Kip1p promotes net shortening of aMTs as a function of motor concentration, which is consistent with the model of Kip1p as a promoter of MT disassembly that acts preferentially on kMTs over iMTs in the nucleus and that also acts on aMTs in the cytoplasm. In addition, Kip3p also acts as a depolymerase, although its activity is preferentially directed toward aMTs and iMTs rather than kMTs, which is consistent with the previous findings in *S. cerevisiae* (Gardner *et al.*, 2008).

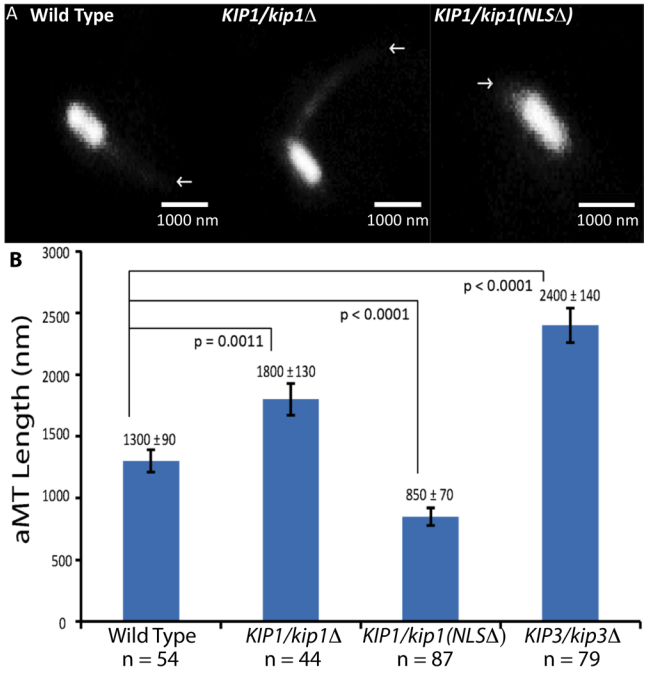

FIGURE 5: Kip1p and Kip3p promote aMT shortening in *C. albicans* yeast. (A) WT aMT, background subtracted for contrast. Arrows represent the end of the associated aMTs. Left to right, WT *Tub1-GFP/tub1 Mtw1-mCherry/mtw1*, *KIP1/kip1Δ Tub1-GFP/tub1 Mtw1-mCherry/mtw1*, and *KIP1/kip1(NLSΔ) Tub1-GFP/tub1 Mtw1-mCherry/mtw1* (strains used were YJB12377, YJB12711, and YJB13143, respectively). (B) Average aMT lengths in WT, *KIP1/kip1Δ*, *KIP1/kip1(NLSΔ)*, and *KIP3/kip3Δ* cells. Average aMT length varies inversely with the expected concentration of motor in the cytosol. The *p* values given were generated using the Student's *t* test (strains used were YJB12377, YJB12711, YJB13143, and YJB13121).

Kip1p-GFP localizes to kinetochore microtubules in the spindle

The length-dependent disassembly model in *S. cerevisiae* predicts that kinesin-5 is associated with kMTs (Gardner *et al.*, 2008). In particular, as motors attach to kMTs and move toward the kMT plus ends, their concentration should rise as they approach the kinetochore, at which point they would promote catastrophe, leading to motor release back into the nucleoplasmic pool. Accordingly, *C. albicans* Kip1p/Kip1p-GFP cells have a bilobed distribution, consistent with its localization on kMTs (Figure 6). The Kip1p-GFP distribution was shifted toward the SPB relative to the kinetochore marker Cse4-GFP (Figure 6C). This is explained in the self-organized model by dissociation of motors from kMT plus ends that shorten past the position of the motors.

Kip3p-GFP localizes to the spindle equator

In contrast to kinesin-5, which is predicted to act preferentially on kMTs due to its tetrameric structure, kinesin-8 homodimers are predicted to preferentially localize to and act on iMTs due to the larger number of binding positions on longer MTs. Most of the Kip3p motors should be found near the iMT plus ends because they are plus end–directed, processive motors (Gupta *et al.*, 2006; Varga *et al.*, 2006). Because iMTs are generally longer than kMTs, the model

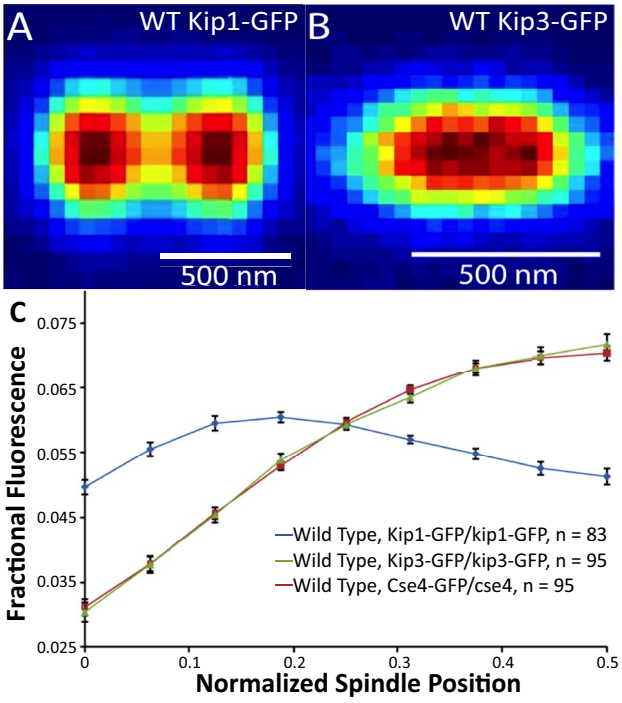

FIGURE 6: Kip1p motors localize to kMTs proximal to kinetochores, and Kip3p motors localize to the spindle equator, in *C. albicans* yeast. (A) Heat map composite image of fluorescence intensity for WT Kip1p-GFP showing that motors localize to kMTs (36 cells; strain used was YJB12162). (B) Heat map composite image of fluorescence intensity for WT Kip3p-GFP showing that motors localize to the spindle midzone (25 cells; strain used was YJB13209). (C) Average fluorescence intensity distribution for Kip1p-GFP and Kip3p-GFP relative to WT Cse4-GFP. The Kip1p-GFP distribution is shifted toward the SPB relative to the kinetochores, and the Kip3p-GFP distribution is localized to the spindle midzone (strains used were YJB12162, YJB13209, and YJB8675).

predicts that Kip3p-GFP fluorescence should be more intense around the spindle equator than Kip1p-GFP fluorescence (see Figure 5A in Gardner *et al.*, 2008). Indeed, on metaphase spindles, WT Kip3p-GFP did not show the bilobed distribution seen for Kip1p-GFP, and instead Kip3p-GFP localized to the spindle equator during metaphase (Figure 6, B and C). This suggests that the dimeric Kip3p motors localize to the iMTs and is consistent with the model prediction that the kinesin-8 dimeric motors will preferentially bind to iMTs and tetrameric motors will bind to the kMTs (Gardner *et al.*, 2008). Accordingly, *KIP3/kip3Δ* spindles also were not obviously disorganized, and the observed motor distribution suggests that Kip3p did not have a significant effect on kMT length regulation. It follows that the in vitro depolymerase activity observed for Kip3p (Varga *et al.*, 2006) may be helping to regulate iMT length, which would account for the increased spindle length in the *KIP3/kip3Δ* spindles (Supplemental Figure S2). Furthermore, the reduced amounts of Kip3p will result in longer iMTs, which provide more MT overlap for Kip1p to cross-link and slide the SPBs apart.

S. cerevisiae Cin8p rescues *C. albicans* KIP1/kip1Δ phenotype

Although the mitotic mechanisms of *S. cerevisiae* and *C. albicans* are similar, there are several important differences between their respective spindle structures. First, the budding yeast metaphase spindle is nearly twice as long as the *C. albicans* metaphase spindles (~1.5 µm; Gardner *et al.*, 2005; Straight *et al.*, 1998) vs. ~0.84 µm (this study), and the kMT plus-end distribution is shifted poleward in budding yeast relative to *C. albicans*, suggesting that the kMTs are slightly shorter relative to the spindle length in budding yeast (see Figure 2A in Gardner *et al.*, 2008). *S. cerevisiae* has two functionally redundant kinesin-5 motors (Cin8p and Kip1p), and Cin8p appears to be more important than ScKip1p in mitosis, as *cin8Δ* mitotic phenotypes are more severe than *kip1Δ* phenotypes, and *S. cerevisiae CIN8 kip1Δ* spindle lengths were more similar to WT than were *cin8Δ KIP1* spindle lengths (Hoyt *et al.*, 1992; Roof *et al.*, 1992; Saunders *et al.*, 1997; Hildebrandt and Hoyt, 2000; Tytell and Sorger, 2006; Gardner *et al.*, 2008).

As indicated by its name, Kip1p is the only kinesin-5 homologue in *C. albicans*, and it is more similar to ScKip1 than to ScCin8p. We reasoned that the differences in the budding yeast and *C. albicans* spindles might be due to *C. albicans* having two copies of *Kip1* rather than single copies of both *Kip1* and *Cin8* (Chua *et al.*, 2007). If ScCin8p is an intrinsically more effective length-dependent depolymerase than ScKip1p, then the self-organized model would predict that cells containing only Kip1p would have shorter spindles with longer kMTs relative to the spindle length than cells containing both Cin8p and Kip1p in equivalent amounts. To test this, we reengineered ScCin8 for *C. albicans* codon usage and constructed a strain heterozygous for CaKip1 and containing a copy of *ScCin8* under native promoters (*KIP1/kip1Δ+CIN8*).

The *S. cerevisiae* kinesin-5 motor Cin8p rescued the *KIP1/kip1Δ* phenotype in *C. albicans*, showing a clear bilobed Tub1-GFP fluorescence distribution characteristic of WT metaphase spindles (Figure 7). This demonstrates that, when expressed from a native *C. albicans* promoter, ScCin8p is not functionally different from CaKip1p and that these highly conserved motors have functionality beyond their species of origin. Furthermore, spindle length of the *KIP1/kip1Δ+CIN8* strain was indistinguishable from that of WT spindles (820 ± 10 nm [±SEM]; $p = 0.15$; Student's *t* test), which is significantly longer than the *KIP1/kip1Δ* spindle length ($p < 0.0001$; Student's *t* test). Thus the presence of ScCin8p in *S. cerevisiae* is not sufficient to explain the differences between the metaphase spindle lengths of *S. cerevisiae* and *C. albicans*. This is consistent with spindle length being determined largely by iMTs rather than by kMTs and thus largely under the control of Kip3p and not Kip1p and/or Cin8p. The *KIP1/kip1Δ+CIN8* spindles had a Tub1-GFP fluorescence intensity distribution that is qualitatively similar, although not identical, to WT ($p = 7 \times 10^{-4}$) and different from the *KIP1/kip1Δ* distribution ($p < 0.0001$). We conclude that ScCin8 can replace Kip1 for establishing the bilobed spindle structure characteristic of wild-type cells and, to a large degree, for spindle length.

KIP1/kip1Δ spindles have longer MTs than WT as measured from electron tomography reconstructions

To assess whether the spindle ultrastructure in *C. albicans* is similar to that previously observed in *S. cerevisiae* (Winey *et al.*, 1995; O'Toole *et al.*, 1999), we performed ET reconstructions of WT and *KIP1/kip1* spindles. ET reconstruction of two WT and three *KIP1/kip1Δ* spindles allowed the individual MTs in each spindle to be visualized (Figure 8A). The MTs in the WT spindles were on average shorter relative to the spindle length (230 ± 26 nm, which represents 20 ± 2% of the spindle length) than those of the *KIP1/kip1Δ* spindles (292 ± 22 nm; 40 ± 3%; $p = 0.011$; chi-squared test; Figure 8B and Table 2). The *KIP1/kip1Δ* spindles also had more MTs that were >50% of the total spindle length (34.4% of all MTs, $n = 122$) than the WT spindles (19.8% of all MTs, $n = 91$; $p = 0.028$; chi-squared test). As with *S. cerevisiae*, the chromosomes do not

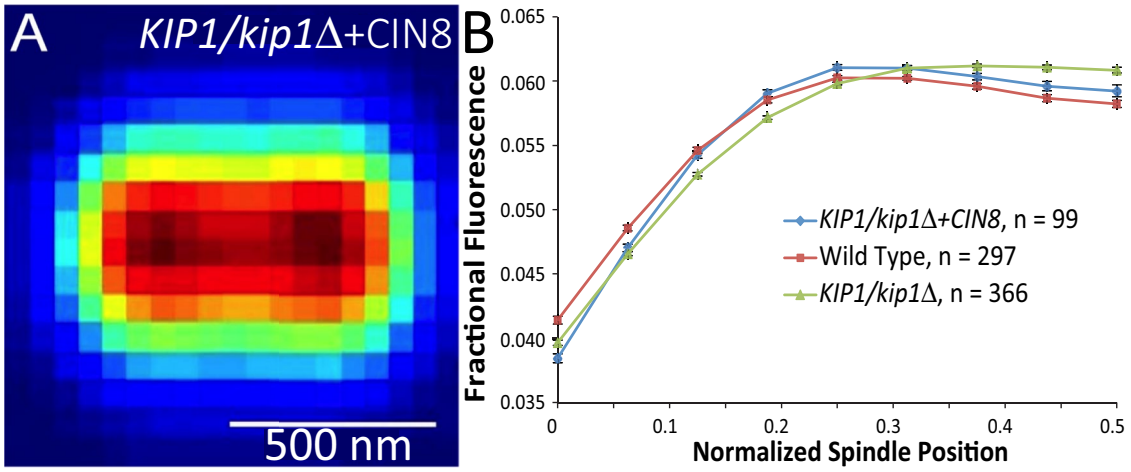

FIGURE 7: *S. cerevisiae* Cin8p rescues the Kip1p heterozygous phenotype in *C. albicans* yeast. (A) Image overlay of fluorescence intensity for *KIP1/kip1Δ+CIN8* spindles showing bilobed fluorescence distribution (33 cells; strain used was YJB13203). (B) Average fluorescence intensity distribution for *KIP1/kip1Δ+CIN8* spindles is qualitatively similar to the WT Tub1-GFP fluorescence distribution (although still statistically different from WT, $p = 7 \times 10^{-4}$) and is different from the *KIP1/kip1Δ* Tub1-GFP fluorescence distribution ($p < 0.0001$; strains used were YJB12377, YJB12711, and YJB13203)

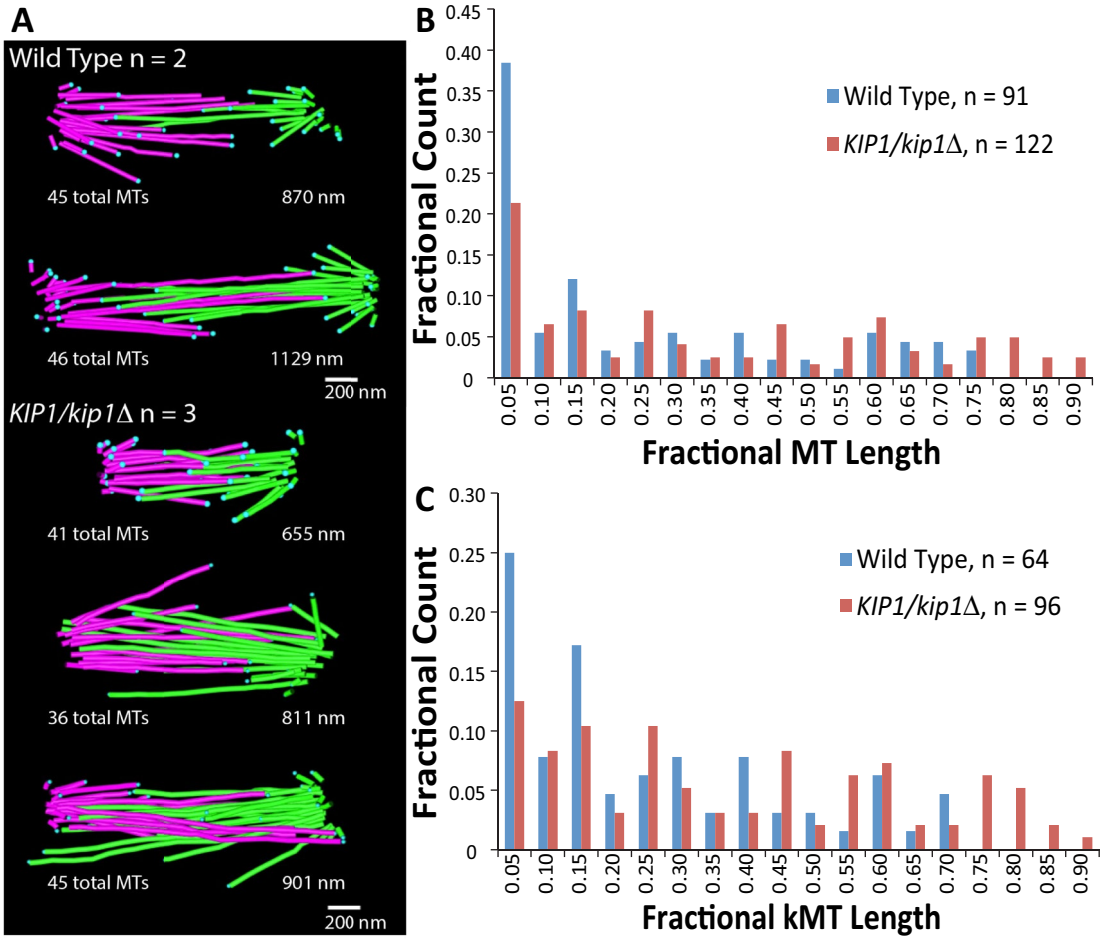

FIGURE 8: ET reconstructions of WT and *KIP1/kip1Δ* spindles show longer, more varied kMTs in the heterozygous mutant spindles in *C. albicans* yeast (note that one WT and one mutant spindle are reproduced from Figure 1). (A) Models of both WT and both *KIP1/kip1Δ* spindles used in EM tomographic analysis with spindle lengths (strains used were YJB12377 and YJB12711). (B) Histogram of MT lengths relative to spindle lengths for WT and *KIP1/kip1Δ* spindles showing shorter WT MTs (strains used were YJB12377 and YJB12711). (C) Histogram of estimated kMT lengths relative to spindle lengths for WT and *KIP1/kip1Δ* spindles showing shorter WT kMTs (strains used were YJB12377 and YJB12711).

	Wild type (870 nm)	Wild type (1129 nm)	*KIP1/kip1Δ* (811 nm)	*KIP1/kip1Δ* (655 nm)	*KIP1/kip1Δ* (901 nm)
Total MTs (SPB 1, SPB 2)	45 (21, 24)	46 (24, 22)	36 (21, 15[a])	41 (21, 20)	45 (22, 23)
Total kMTs (assume)	32	32	32	32	32
Mean MT length (nm)	188 ± 26	272 ± 44	381 ± 38	170 ± 22	331 ± 44
Mean MT length (fraction of spindle length)	0.2 ± 0.03	0.2 ± 0.04	0.5 ± 0.05	0.3 ± 0.03	0.4 ± 0.05
Mean kMT length (nm)	189 ± 25	282 ± 46	339 ± 36	165 ± 23	354 ± 44
Mean kMT length (fraction of spindle length)	0.2 ± 0.03	0.2 ± 0.04	0.4 ± 0.04	0.3 ± 0.03	0.4 ± 0.05

[a]Incomplete reconstruction.

TABLE 2: EM spindle statistics.

condense to a structure that can be visualized in the electron microscope (EM) to identify which MT is a kMT. However, the EM reconstructions show that there are sufficient numbers of MTs for 1 MT/kinetochore, so the majority of MTs are likely kMTs, whereas a relatively small fraction (~10%) are iMTs. Assuming that both the WT and *KIP1/kip1Δ* spindles have the same number of iMTs, this suggests that more MTs cross the spindle equator in the *KIP1/kip1Δ* spindles, which is consistent with the *KIP1/kip1Δ* spindles having longer and less organized MTs than WT, as is predicted by the self-organized assembly model.

Assuming that there are four iMTs/spindle during metaphase (two per SPB) and 1 kMT/chromatid (32 total kMTs; Joglekar *et al.* 2008), we see that the kMT length distributions of the EM spindles were generated by removing the four longest MTs and then removing the shortest MTs until there were 32 MTs left (Figure 8C). Even in the absence of the longest MTs, the *KIP1/kip1Δ* spindles have longer kMTs and more kMTs that cross the spindle equator (>50% of the spindle length) than the WT spindles. This is in direct agreement with the Cse4-GFP fluorescence data, which show that in WT cells, the kinetochores are clustered around the spindle equator, suggesting that only a small number of kMTs cross the spindle equator. This is also in agreement with the Tub1-GFP fluorescence data, which show an increase in fluorescence intensity at the spindle equator in the *KIP1/kip1Δ* spindles relative to the WT spindles and is consistent with the self-organized assembly model.

These EM results support our findings obtained by fluorescence microscopy that deletion of one copy of Kip1p leads to longer kMTs and thus less-organized spindles than in WT. However, due to very small sample sizes and spindle-to-spindle variability, it is difficult to draw specific conclusions about kMT length and spindle organization from the EM data alone. Nevertheless, the EM provides independent experimental confirmation of the basic structure of the spindle and lengths of MTs inferred from fluorescence microscopy.

Simulating CaKip1-mediated, length-dependent kMT assembly dynamics

Computational modeling of the length-dependent disassembly model of kinesin-5 allowed the model to be explicitly tested against the experimental data for *C. albicans*. In the Monte Carlo simulation (Gardner *et al.*, 2008), kMT and iMT dynamics could be tracked as kinesin-5 motors progressed along their lengths toward MT plus ends and promoted catastrophe when they reached them. The computer simulation of the kMT dynamics in *C. albicans* is based on the previously described tension-dependent rescue model (Sprague *et al.*, 2003) and the motor-dependent catastrophe model (Gardner *et al.*, 2008).

Our simulation was tested by reconstructing the *S. cerevisiae* model described in Gardner *et al.* (2008) and verifying our results against those previously described (Figure 9, A and B). The simulation parameters were then adjusted to fit the observed *C. albicans* spindle length and distribution (all simulation parameters are listed in Supplemental Table S3). The intersection of the catastrophe and rescue frequencies forms attractor zones of kinetochore microtubule plus ends, where microtubules have a zero net growth rate ($V_g = 0$). With a strong catastrophe gradient due to a large number of kinesin-5 motors, the attractor zone is located approximately midway between the spindle pole and spindle equator (Figure 9, catastrophe and rescue frequencies). As expected, the plus ends of kinetochore microtubules cluster at these locations on both sides of the spindle equator (Figure 9, histograms). Reducing the number of motors leads to a weaker catastrophe gradient, pushing the attractor zone closer to the equator. This results in kinetochore microtubules that are both longer and more variable in length. These results are consistent with both *S. cerevisiae* WT (more motors) and *cin8Δ* (reduced motors) and *C. albicans* WT (more motors) and *KIP1/kip1Δ* (reduced motors), despite the difference in spindle lengths between the two organisms. In both cases, by changing only the number of motors, the model demonstrates that kMT plus ends fail to congress properly due to a decrease in catastrophe frequency (Figure 9). Thus the lack of kinesin-5 motors is sufficient to explain the observed spindle organization using the motor-dependent catastrophe model.

Estimation of CV for congression in the *C. albicans* mitotic spindle

From the simulation parameters, we can estimate the coefficient of variation of kMT lengths in the *C. albicans* spindle, which was predicted to be >0.43, based on the comparison to *S. cerevisiae* described earlier. Because the experimental data for WT shown earlier exhibit the hallmarks of a congressed spindle, the CV should be <1.0, which is the value obtained for random positioning of kinetochores within the spindle. Using the *C. albicans* WT parameter values in Supplemental Table S3, we estimate V = 1.2 μm/min and $\beta = 20\ \mu m^{-1}\ min^{-1}$. On the basis of the tubulin fluorescence distribution, we can estimate the mean kMT length by the position at which the decrease of fluorescence is steepest, ~0.4, which, when multiplied by the spindle length, 840 nm, gives $\langle L \rangle$ = (0.4)(840 nm) = 336 nm. At this length, $k_c = k_r = 8.7\ min^{-1}$ for $\tau = 0.11$ min (6.9 s). Putting these values together, we obtain, via Eq. S31 in the Supplemental Material, Pe = 4.9. From Eq. 2, the CV is estimated to be

$$\frac{\sigma}{\langle L \rangle} = \sqrt{\frac{2}{4.9}} = 0.64 \qquad (4)$$

or, equivalently, SNR = 1.56. Thus we estimate the SD of kMT lengths to be σ = (0.64)(336 nm) = 215 nm. For the *C. albicans KIP1/kip1Δ*, we estimate, using the same approach, that Pe = 4.8, which

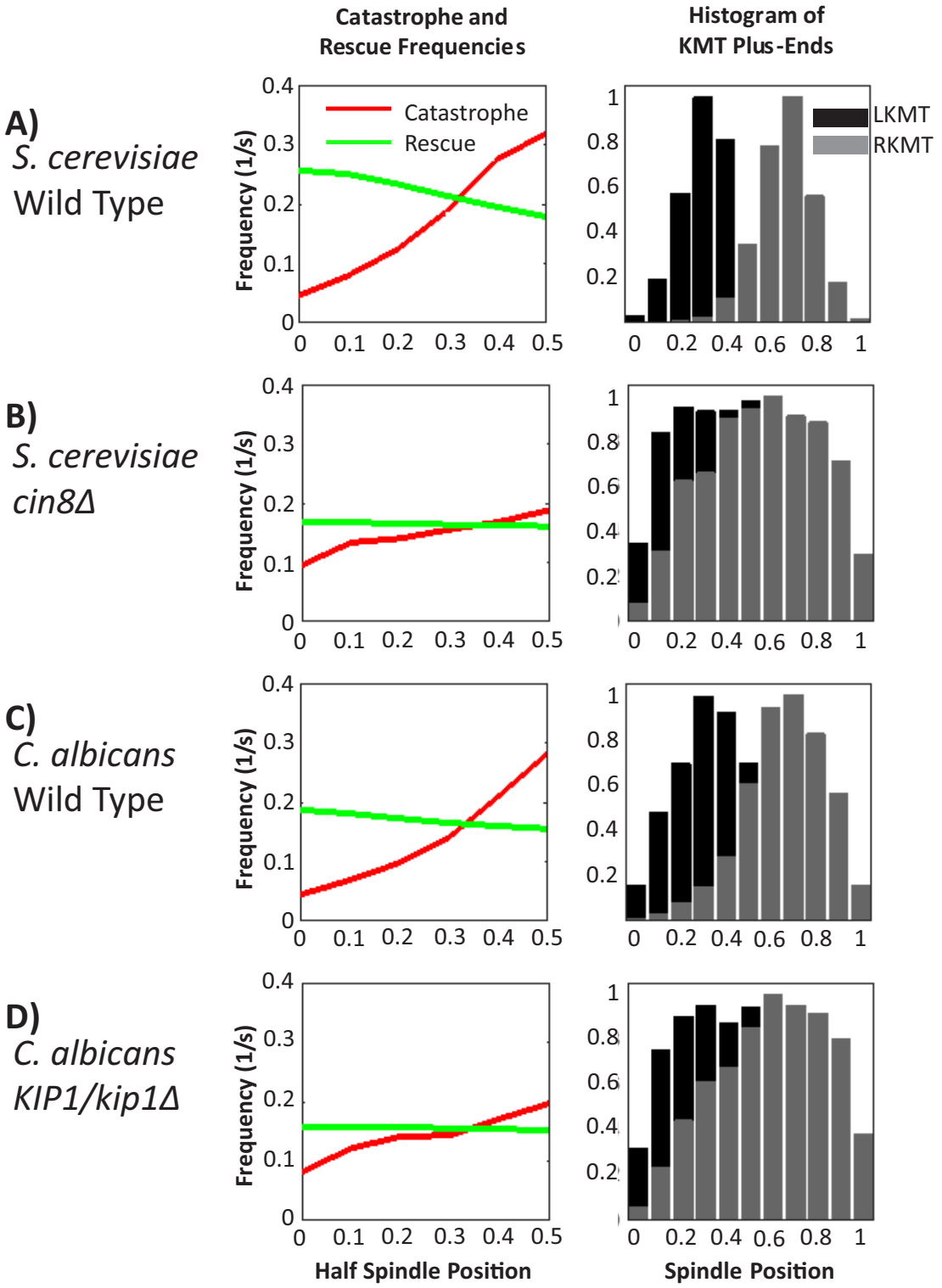

FIGURE 9: Simulated kinetochore microtubule catastrophe and rescue frequencies based on spindle position and histogram of plus-end positions for *S. cerevisiae* and *C. albicans* WT and mutant parameter sets. Attractor zones formed by the intersection of catastrophe and rescue frequencies indicate approximate mean location of kMT plus ends. LKMT denotes kinetochore microtubules that grow from the left spindle pole; RKMT denotes kinetochore microtubules that grow from the right spindle pole. (A) *S. cerevisiae* WT shows an attractor zone located midway between the spindle pole and the equator and tight clustering of plus ends at this location on either side of the spindle equator. (B) *S. cerevisiae cin8*Δ shows a weaker catastrophe gradient relative to WT, which leads to a weaker attractor zone, longer and more variable kinetochore microtubule lengths, and thus weaker clustering of plus ends. (C) *C. albicans* WT shows an attractor zone located slightly closer to the spindle equator compared with *S. cerevisiae* WT, leading to clustering of plus ends closer to the equator. (D) *C. albicans KIP1/kip1*Δ shows a weaker catastrophe gradient relative to WT, which leads to a weaker attractor zone, longer and more variable kinetochore microtubule lengths, and thus weaker clustering of plus ends, as in *S. cerevisiae cin8*Δ.

yields CV = 0.65 and SNR = 1.55, with $\langle L \rangle = 383$ nm and $\sigma = 247$ nm. Thus the kinetochores are less congressed due to kMTs being longer and more variable in length than WT.

DISCUSSION

Collectively our results demonstrate that precise, submicrometer control of kMT lengths and chromosome congression is achieved in *C. albicans*, whose mitotic spindle is among the smallest of known eukaryotic spindles (measured here as ~840 nm). Similar-sized and smaller spindles exist among the eukaryotes, including green algae (600–800 nm; Gan *et al.*, 2011; Supplemental Figures S3 and S4). However, these microorganisms lack sufficient numbers of microtubules to achieve a minimal 1:1 coupling of microtubules to chromosomes and so likely segregate chromosomes by an alternative, unknown mechanism. By contrast, based on our analysis, *C. albicans* has sufficient numbers of microtubules to achieve a minimal 1:1 coupling of kMTs to kinetochores. Thus our results show that despite the myriad of putative exotic mitotic mechanisms among phylogeny (Drechsler and McAinsh, 2012), a submicrometer-length mitotic spindle can exhibit the "classic" congressed spindle organization commonly associated with larger spindles.

From our analysis, we can now establish a simple scaling relationship that defines the CV as function of spindle length. As shown in Figure 10, using the foregoing calculated numbers, we find that the CV increases with decreasing spindle length. By empirically fitting a power-law relationship using the two shortest spindles (*S. cerevisiae* and *C. albicans*) given by

$$\mathrm{CV} = a \cdot \mathrm{SL}^{b} \tag{5}$$

where SL is the spindle length (in micrometers), we estimate $a = 0.57$ and $b = -0.61$. As shown in Figure 10, this means that the data reveal a nearly inverse square-root relationship between CV and SL. The relationship allows us to estimate the lower bound for "classic" eukaryotic spindle length by substituting CV = 1 into Eq. 5, and we obtain

$$\mathrm{SL}(\mathrm{CV} = 1) = 0.4\ \mu\mathrm{m} \tag{6}$$

Assuming that αβ-tubulin heterodimers, the fundamental subunits that self-assemble to form microtubules, are 8 nm in length, we find that the lower bound corresponds to 50 dimer layers. For a spindle at the lower limit, where CV = 1, this means an average kMT length of at most half this length, 0.20 μm, or 25 dimer layers. In this limit, kinetochores would be nearly uniformly distributed along the spindle axis, with no semblance of congression. It is interesting to note that, to our knowledge, there are no spindles shorter than this lower limit. The only known spindle shorter than that of *C. albicans* is possibly that of the unicellular green algae *Ostreococcus tauri*, the smallest known eukaryote, which appears to have a spindle length of ~0.5 μm (Gan *et al.*, 2011). However, the *O. tauri* spindle lacks sufficient numbers of microtubules to match the numbers of chromosomes and so is believed to not conform to the classic spindle structure (Gan *et al.*, 2011). We speculate that even above the lower limit (e.g., ~0.5 μm for *O. tauri*), congression would be difficult to achieve, and so alternative strategies may be required to achieve high-fidelity genome segregation. In general, organisms such as *O. tauri* and *C. albicans* challenge the fundamental lower limits of spindle organization in the context of nanometer-scale microtubule assembly "noise," whereas typical animal spindle lengths are ~10 μm and can be as large as 60 μm (Goshima and Scholey, 2010). It appears that *C. albicans* has the smallest known spindle that maintains sufficient MT numbers to achieve at least 1:1 coupling to kinetochores and that spatial control of kMT length on the nanoscale necessary for congression is largely ensured by the kinesin-5, Kip1p, rather than the kinesin-8, Kip3p.

Our results are consistent with a mechanism by which kinesin-5 regulates chromosome congression via length-dependent depolymerase activity in *C. albicans*, consistent with the Gardner *et al.* (2008) self-organized model of kMT length regulation in budding yeast. Longer kMTs are more likely to undergo net shortening, most likely through catastrophe, due to the increased number of kinesin-5 motors that can bind to them, thus suppressing net kMT assembly when the kMT plus ends are near the equator, and centering the plus-end associated chromosomes near the spindle equator. In cells lacking kinesin-5 in the nucleus (*KIP1/kip1Δ* and *KIP1/kip1(NLSΔ)*), the spindles do not display the same level of kMT organization as the WT cells. EM reconstructions of both WT and *KIP1/kip1Δ* spindles confirm the longer and more disorganized kMTs in the *KIP1/kip1Δ* spindles inferred from the fluorescence microscopy images of Tub1-GFP. The net longer and more variable-length kMTs suggest that the chromosomes are not properly congressed at the spindle equator during metaphase in mutant cells. Note that the EM data cannot unambiguously discriminate between kMTs and iMTs; however, based on Joglekar *et al.*'s (2008) estimate of 2 iMTs/SPB and 1 kMT/kinetochore, the majority of the ~45 MTs/spindle observed (Table 2) must be kMTs. This means that with the elimination of

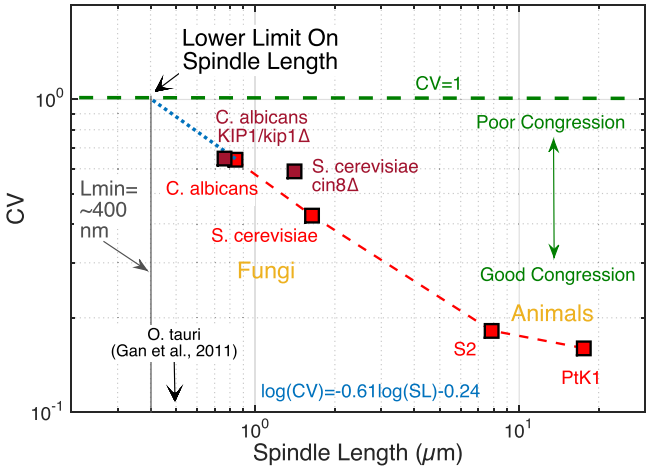

FIGURE 10: Scaling analysis sets a lower limit on spindle length in congressed eukaryotic spindles. Four wild-type spindles of various lengths are plotted in terms of their CV. When CV = 1, spindles are not congressed, but as CV decreases, congression quality improves. For the two shortest spindles, a power-law relationship (exponent $b = -0.61$) approximately describes CV as a function of spindle length (SL; the equation shown is the log-transformed form of Eq. 5). When CV = 1, this inverse relationship predicts a minimum spindle length of 404 nm (equivalent to ~50 αβ-tubulin dimer lengths). The smallest known eukaryote, *O. tauri*, has a spindle length of ~0.5 μm (Gan *et al.*, 2011) but lacks sufficient numbers of microtubules to achieve the minimal 1:1 coupling of kinetochores to microtubules, as illustrated in Figure 1. Mutations in kinesin-5 in both *S. cerevisiae* (Gardner *et al.*, 2008) and *C. albicans* (this study) are sufficient to increase CV with modest decrease in SL, meaning that kinesin-5 mediates congression in both yeast organisms. Animal spindles have a CV that is only weakly dependent on spindle length and may plateau, ~CV = 0.15. Data for *C. albicans* and S2 cells are from the present study, data for *S. cerevisiae* are from Gardner *et al.* (2008), and data for PtK1 cells are from Cimini *et al.* (2004).

extreme lengths (~4 longest and 8 or 9 shortest MTs), we are left with what are primarily kMTs.

In *S. cerevisiae*, kinesin-5 cross-links antiparallel iMTs and provides a force that pushes the spindle pole bodies apart, thus elongating the spindle, an effect that is seen in the shortening of spindles lacking kinesin-5 (*KIP1/kip1Δ* and *KIP1/kip1(NLSΔ)*) and that is particularly important during anaphase. However, the Kip1p-GFP results show that during metaphase, the majority of Kip1p is segregated on either side of the spindle equator, meaning that most kinesin-5 is associated with the kMTs, because iMT-associated Kip1p would be apparent near the spindle equator due to the longer length of iMTs. The close correspondence between the kinetochore distribution and the Kip1p distribution suggests that kinesin-5 directly regulates the kMT length distribution by acting at the kMT plus ends. The presence of a yeast kinesin-5 in the *C. albicans* nucleus during mitosis is sufficient to organize the spindle, regardless of the specific kinesin-5 and its yeast species of origin. The aMT length is dependent on the concentration of Kip1p in the cytosol, further demonstrating that Kip1p has strong depolymerase activity on kMTs and aMTs.

Although this study does not elucidate the mechanism by which kinesin-5 acts as a depolymerase, the most likely mechanism is through direct interaction with the MT plus ends, possibly through disruption of the crystal lattice or GTP cap. Another possible mechanism is that kinesin-5 motors transport a protein responsible for depolymerization to the plus ends. Although kinesin-5 motors are not known to transport cargoes, in budding yeast, the molecular chaperone Sse1 helps to symmetrically distribute Cin8p throughout the spindle, although how this is mechanistically involved with the depolymerase activity of Cin8p is unknown (Makhnevych and Houry, 2013). Similarly, the human kinesin-5, Eg5, has been shown to directly interact with EB1, the MT tip–tracking protein, which raises the possibility that such interactions may play a role in kinesin-5 plus-end activity in higher eukaryotes (Jiang *et al.*, 2012). The extent to which this mechanism is generalized is also unknown, as it has been shown in both budding yeast and *C. albicans*, but it has yet to be demonstrated outside of yeast. The greater number of motors associated with animal spindles may lead to a breakdown of the mechanism or a distribution of the plus-end disassembly activity of yeast kinesin-5 across several motors.

The similarity of the spindles in the *KIP1/kip1Δ+CIN8* background and WT suggests that yeast kinesin-5 motors can function outside of their unique biochemical and species-specific context. Kinesins are highly conserved across species, but this shows that they can function in other species under native promoters, suggesting that their function does not depend on unique biochemical pathways or signaling. This result also demonstrates that there is no functional difference between ScCin8p and CaKip1p, and the presence of Cin8p in *S. cerevisiae* and not *C. albicans* by itself is not sufficient to explain the differences in the spindle length between those two species. In addition, we found that the cell size (yeast vs. hyphal) did not affect spindle size or organization, demonstrating a breakdown of the proposed cell size/spindle size scaling for small cells based on analysis of *Xenopus laevis* cell and spindle size (Mitchison *et al.*, 2012). The shorter spindles present in *C. albicans* are not due to its only having Kip1p, and the origin of that difference is unknown, but it might be due to different kinesin-5 levels in the cell under native promoters or a smaller number of iMTs affecting the force balance of the spindle, or possibly higher levels of tubulin expression in *S. cerevisiae* than in *C. albicans*.

Finally, *C. albicans* and several related yeasts are often aneuploid (carry extra copies of one to a few chromosomes), suggesting that mitosis might be less tightly regulated in these pathogenic fungi than in *S. cerevisiae* (Selmecki *et al.*, 2006, 2010; Harrison *et al.*, 2014). Furthermore, specific aneuploidies can confer resistance to antifungal drugs through altered gene copy numbers present in aneuploidy cells. Our experimental results demonstrate that Kip1, but not Kip3, plays a crucial role in kMT length regulation, which subsequently affects chromosome congression in metaphase. Without proper congression, mitotic errors leading to aneuploidy are more likely. Altering the activity of Kip1p might serve as a way to control the degree to which aneuploidy arises and determine whether antifungal resistance results. In addition, the chromosome congression model can be used to predict in silico the parameters that are most and least likely to result in a disorganized spindle leading to aneuploidy and to map target molecules to model parameters. Thus an interesting alternative approach to targeting antifungal resistance is to focus on fungal-specific aspects of mitosis as potential targets for new therapeutic antifungal strategies.

MATERIALS AND METHODS

Yeast strains and cell cultures

All strain descriptions are given in Table 3, all oligonucleotides are listed in Supplemental Table S1, and all primers used are listed in Supplemental Table S2. Cells were cultured on solid synthetic defined yeast culture (SDC) medium on 1% agar plates and incubated at 30°C. Cells were prepared for imaging in 2% glucose liquid SDC medium and incubated in an orbital shaker for ~2 h at 30°C/225 rpm

Strain number	Genotype	Source
RM1000	*ura3::imm434/ura3::imm434 iro1/iro1::imm434 his1::hisG/his1::hisG*	Alonso-Monge *et al.* (2003)
BWP17	*ura3::imm434/ura3::imm434 iro1/iro1::imm434 his1::hisG/his1::hisG arg4/arg4*	Wilson *et al.* (1999)
YJB8599	*BWP17 TUB1-GFP-HIS1/TUB1*	Burrack *et al.* (2011)
YJB8675	*BWP17 CSE4/CSE4:GFP:CSE4*	Joglekar *et al.* (2008)
YJB12162	*RM1000 KIP1/KIP1-GFP-NAT1*	This work
YJB12377	*YJB8599 MTW1/MTW1-mCherry-NAT1*	This work
YJB12711	*YJB12377, KIP1/kip1::ARG4*	This work
YJB12859	*BWP17 TUB4/TUB4-mCherry*	This work
YJB13092	*YJB12162 TUB1/TUB1-mCherry-URA3*	This work
YJB13121	*YJB12377 kip3::ARG/KIP3*	This work
YJB13143	*YJB12377 KIP1/kip1-nls1Δ*	This work
YJB13180	*YJB12859 MTW1-GFP/MTW1*	This work
JLR48/YJB13190	*SC5314 cch1::frt/cch1::frt*	Reedy *et al.* (2010)
YJB13196	*YJB8675 TUB4:mCherry/TUB4*	This work
YJB13203	*YJB12711 + codon optimized ScCIN8*	This work
YJB13209	*KIP3/KIP3-GFP*	This work

TABLE 3: *C. albicans* strains used in this study.

for the budding yeast morphology experiments and 37°C/225 rpm for hyphae experiments. For hyphae experiments, before incubation in the shaker, the cells were incubated at 30°C in 2% glucose SDC medium overnight and then diluted 1:50 in SDC medium containing 10% adult bovine serum and 2% glucose. For imaging, 10 µl of cell suspension was plated on a polyethylenimine-coated, 35-mm dish with a round, 14-mm, no. 1.5 coverglass bottom (P35G-1.5-14-C; MatTek, Ashland, MA), allowed to adhere to the dish for 10 min, and covered with polydimethylsiloxane oil to limit dehydration.

Strain construction

Strain YJB12377 was constructed by transforming YJB8599 with a PCR product amplified from pMG2343 (pMcherry-*NAT*) and primers 5033 and 5034, and the correct 1.2-kbp fragment was confirmed by PCR with oligonucleotides 2717 and 4036. YJB12711 was constructed by transforming YJB12377 with the 2.1-kb amplification product from pGEM-*ARG4* using primers 4368 and 4369. The PCR product was transformed into strain YJB12377 (Tub1-GFP, Mtw1-mCherry), and the correct 1.5-kb product was detected by amplification with primers 4371 and 730. We were not able to directly measure Kip1 copy number in this *KIP1/kip1Δ* strain (YJB12711). However, its spindle phenotype and the fact that it was complemented with *ScCIN8* (in YJB13203) are consistent with the idea that the Kip1 protein concentration is reduced in YJB12711. YJB12162 was constructed by transforming RM1000 with a 3.9-kbp PCR product amplified from pMG2120 and primers 4732 and 4733, and the transformants were screened by PCR with oligonucleotides 658 and 4734 for a 872–base pair product, and the GFP fusion was confirmed by DNA sequencing. YJB13092 was constructed by transforming YJB12162 with the 3.0-kbp PCR product amplified from pMG2254 and primers 5838 and 5839. Transformants were selected on SDC-Ura and confirmed by PCR amplification of a 1.2-kbp product with primers 944 and 1434. YJB13121 was constructed by transforming YJB12377 with the 2.1-kbp PCR product amplified from pGEM-*ARG4* and primers 6042 and 6043. Transformants were selected on SDC-Arg and confirmed by PCR amplification of an 820–base pair product with primers 6044 and 1251 and a 1.7-kbp product with primers 730 and 6045. We were unable to directly measure Kip3 copy number in this *KIP3/kip3Δ* strain (YJB13121). Once again, however, its spindle phenotype is consistent with the idea that the Kip3 protein concentration was reduced in this strain. YJB13143 was constructed by transforming YJB12377 with the 1.6-kbp PCR product amplified from pGEM-*URA3* and primers 6056 and 6057. Transformants were selected on SDC-URA and confirmed by PCR amplification of a 1.2-kbp product with primers 944 and 5624 and a 3.3-kbp product with primers 5621 and 945. YJB12859 was constructed by transforming BWP17 with the PCR product amplified from pMG2343 and primers 5345 and 4311. Transformants were selected on yeast extract–peptone–dextrose medium + adenine (YPAD) + nourseothricin (NAT) and confirmed by PCR amplification of a 1-kbp product with primers 3326 and 4313. YJB13180 was constructed by transforming YJB12859 with the 3.7-kbp PCR product amplified from pMG1646 and primers 2715 and 4266. Transformants were selected on SDC-His and confirmed by PCR amplification of a 1.1-kbp product with primers 2717 and 658. YJB13196 was constructed by transforming YJB8675 with the 3.1-kbp PCR product amplified from pMG2254 and primers 4311 and 4312. Transformants were selected on SDC-Ura and confirmed by PCR amplification of a 1.0-kbp product with primers 4313 and 4036. YJB13203 was constructed by transforming YJB13196 with the 2.8-kbp PCR product amplified from pGEM-*HIS1* and primers 4368 and 4369. Transformants were selected on SDC-His and confirmed by PCR amplification of a 1.6-kbp product with primers 565 and 4370 and a WT allele with primers 5033 and 4371. YJB13209 was constructed by transforming YJB12859 with the 3.2-kbp PCR product amplified from pMG1602 and primers 6158 and 6159. Transformants were selected on SDC-Ura and confirmed by PCR amplification of a 450–base pair product with primers 725 and 6045.

Fluorescence imaging

All live-cell fluorescence images were collected on a Nikon (Melville, NY) TE200 inverted microscope with a 60×, 1.49 numerical aperture (NA) Plan Apo objective with a 2.5× projection lens, illuminated with the 89 North PhotoFluor II light source, and detected with an EGFP/mCherry ET (59022; Chroma Technology, Bellows Falls, VT) filter set. The images were collected on a 1390 z 1040 14-bit CoolSnap *HQ*^{2} charge-coupled device (CCD) camera with ~60% quantum efficiency (Photometrics,Tucson, AZ). One hundred percent illumination from the light source was used, and the exposure times varied from 100 to 500 ms for GFP and 100 to 800 ms for mCherry, depending on the experiment, controlled via a shutter (Uniblitz, Rochester, NY). All images collected were single plane and at a single time point. The imaging system was controlled by MetaMorph software (Molecular Devices, Sunnyvale, CA), and the cells were incubated on the stage at room temperature.

Electron tomography

Cells were prepared for electron microscopy using high-pressure freezing and freezing substitution as essentially described in Winey *et al*. (1995). Dual-axis tilt series acquisition was carried out using a Tecnai TF30 (FEI, Hillsboro, OR) operating at 300 kV (O'Toole *et al*., 2002). Tomographic reconstruction and modeling of spindle MTs was performed using the IMOD software package (Kremer *et al*., 1996). The lengths of spindle MTs were measured from the model contour data using the program IMODINFO within the IMOD package.

Image analysis

Mitotic spindles were determined to be in metaphase based on a length criterion. Once the spindles form, the cell remains in a metaphase steady state for ~60 min (Supplemental Figure S1B) until the spindle rapidly elongates during anaphase (Yeh *et al*., 1995; Burke and Stukenberg, 2008). It was assumed that the majority of visible spindles would be in metaphase for this reason, so the metaphase length (as measured from SPB to SPB) was determined by taking the mean length of all spindles. Metaphase spindles were defined as spindles that were within 1 SD of the mean. Cells that fell outside this criterion were assumed to likely either be in prometaphase if they were too short or anaphase if they were too long.

The collected images were analyzed using a MATLAB (MathWorks, Natick, MA) script that calculated the average fluorescence distribution over the normalized half-spindle. The MT minus ends were located using the Gaussian survival function method in the tip-tracking code as previously described (Demchouk *et al*., 2011), and line scans were taken along the length of the rotated spindle to determine the average fluorescence intensity at each point along the spindle, which was then normalized to 0.5 for the half-spindle. The astral microtubule lengths were calculated by manually selecting the location of the plus and minus ends in the image and calculating the distance between the two points.

Simulation methods

Monte Carlo simulations were run using MATLAB based on methods described previously (Sprague *et al*., 2003; Gardner *et al*., 2005,

2010; Gardner and Odde, 2010). Briefly, for *C. albicans* spindles, 32 kMTs (16 from each SPB) were simulated to allow each of the eight diploid chromosomes (i.e., 16 replicated chromosomes, for a total of 32 sister chromatids) a single attachment to each pole, and four total iMTs (two from each SPB) were simulated (Joglekar *et al.*, 2008). The spindle length was fixed at 840 nm to match the observed experimental mean spindle length (837 ± 8 nm; see *Results*) for the WT and 766 nm for the *KIP1/kip1Δ* simulation. As described in Sprague *et al.* (2003), only the plus ends of the MTs were allowed to undergo dynamic instability because the majority of kMT dynamics takes place at the plus end (Maddox *et al.*, 2000; Gardner *et al.*, 2005), and the minus ends were fixed at the SPBs. Thirty motors were used to simulate WT conditions and 10 to simulate *KIP1/kip1Δ* conditions. All simulations started with no initial motor attachments. All parameters for both conditions are given in Supplemental Table S3. Parameters for the *S. cerevisiae* simulations were taken directly from Gardner *et al.* (2008).

All other simulation details were previously described (Sprague *et al.*, 2003, Gardner *et al.*, 2005, 2008, 2010; Gardner and Odde 2010).

Measuring spindle lengths and kinetochore microtubule lengths in *Drosophila* S2 cells and PtK1 cells

Nonadherent *Drosophila* S2 cells were maintained in culture in T25 flasks at room temperature in M3 insect medium supplemented with 10% insect medium supplement (IMS) plus 2% fetal bovine serum albumin and 10% penicillin/streptomycin. All cells were imaged on a Zeiss LSM 7 Live swept-field confocal microscope using a 100×/1.45 NA Plan-Fluor oil immersion objective with 488- and 561-nm lasers and 495- to 555-nm and 575- to 615-nm plus long-pass 655-nm filter sets. Images were collected on a 1 × 512 line scanning 12-bit CCD camera with 60% quantum efficiency. Spindle lengths and kinetochore microtubule lengths were measured using the measurement tool in ImageJ (National Institutes of Health, Bethesda, MD). PtK1 cell spindle and kinetochore microtubule lengths were measured using the same approach using data from Figures 2, A and B, and 3, A and B in Cimini *et al.* (2004).

ACKNOWLEDGMENTS

We thank Mark McClellan and Maryam Gerami-Nejad for technical assistance and Mark Winey for his contribution to the EM data. We thank Thomas H. Giddings, Jr., and Christina Clarissa of the Molecular, Cellular, and Developmental Biology EM Suite for freezing and preparing samples for electron microscopy. Electron tomography was performed in the Boulder Laboratory for 3D Electron Microscopy of Cells, which is supported by Grant P41GM103431 from the National Institute of General Medical Sciences to A. Hoenger. This work was funded by National Institutes of Health Grant R01-GM71522 to D.J.O. and National Institutes of Health/National Institute of Allergy and Infectious Diseases Grant AI075096 to J.B.

REFERENCES

Alonso-Monge R, Navarro-García F, Román E, Negredo AI, Eisman B, Nombela C, Pla J (2003). The Hog1 mitogen-activated protein kinase is essential in the oxidative stress response and chlamydospore formation in Candida albicans. Eukaryotic Cell 2, 351–361.

Berman J (2006). Morphogenesis and cell cycle progression in Candida albicans. Curr Opin Microbiol 9, 595–601.

Brand A (2012). Hyphal growth in human fungal pathogens and its role in virulence. Int J Microbiol 2012, 11.

Burke DJ, Stukenberg PT (2008). Linking kinetochore-microtubule binding to the spindle checkpoint. Dev Cell 14, 474–479.

Burrack LS, Applen SE, Berman J (2011). The requirement for the Dam1 complex is dependent upon the number of kinetochore proteins and microtubules. Curr Biol 21, 889–896.

Chua PR, Roof DM, Lee Y, Sakowicz R, Clarke D, Pierce D, Stephens T, Hamilton M, Morgan B, Morgans D, *et al.* (2007). Effective killing of the human pathogen Candida albicans by a specific inhibitor of non-essential mitotic kinesin Kip1p. Mol Microbiol 65, 347–362.

Cimini D, Cameron LA, Salmon ED (2004). Anaphase spindle mechanics prevent mis-segregation of merotelically oriented chromosomes. Curr Biol 14, 2149–2155.

Cole DG, Saxton WM, Sheehan KB, Scholey JM (1994). A "slow" homotetrameric kinesin-related motor protein purified from Drosophila embryos. J Biol Chem 269, 22913–22916.

Demchouk A, Gardner M, Odde D (2011). Microtubule tip tracking and tip structures at the nanometer scale using digital fluorescence microscopy. Cell Mol Bioeng 4, 192–204.

Drechsler H, McAinsh AD (2012). Exotic mitotic mechanisms. Open Biol 2, 120140.

Enos AP, Morris NR (1990). Mutation of a gene that encodes a kinesin-like protein blocks nuclear division in A. nidulans. Cell 60, 1019–1027.

Finley KR, Berman J (2005). Microtubules in Candida albicans hyphae drive nuclear dynamics and connect cell cycle progression to morphogenesis. Eukaryotic Cell 4, 1697–1711.

Gan L, Ladinsky MS, Jensen GJ (2011). Organization of the smallest eukaryotic spindle. Curr Biol 21, 1578–1583.

Gardner MK, Bouck DC, Paliulis LV, Meehl JB, O'Toole ET, Haase J, Soubry A, Joglekar AP, Winey M, Salmon ED, *et al.* (2008). Chromosome congression by kinesin-5 motor-mediated disassembly of longer kinetochore microtubules. Cell 135, 894–906.

Gardner MK, Odde DJ (2010). Stochastic simulation and graphic visualization of mitotic processes. Methods 51, 251–256.

Gardner MK, Pearson CG, Sprague BL, Zarzar TR, Bloom K, Salmon ED, Odde DJ (2005). Tension-dependent regulation of microtubule dynamics at kinetochores can explain metaphase congression in yeast. Mol Biol Cell 16, 3764–3775.

Gardner M, Sprague B, Pearson C, Cosgrove B, Bicek A, Bloom K, Salmon ED, Odde D (2010). Model convolution: a computational approach to digital image interpretation. Cell Mol Bioeng 3, 163–170.

Gatlin JC, Bloom K (2010). Microtubule motors in eukaryotic spindle assembly and maintenance. Seminars Cell Dev Biol 21, 248–254.

Goshima G, Saitoh S, Yanagida M (1999). Proper metaphase spindle length is determined by centromere proteins Mis12 and Mis6 required for faithful chromosome segregation. Genes Dev 13, 1664–1677.

Goshima G, Scholey JM (2010). Control of mitotic spindle length. Annu Rev Cell Dev Biol 26, 21–57.

Gupta ML, Carvalho P, Roof DM, Pellman D (2006). Plus end-specific depolymerase activity of Kip3, a kinesin-8 protein, explains its role in positioning the yeast mitotic spindle. Nat Cell Biol 8, 10.

Hagan I, Yanagida M (1990). Novel potential mitotic motor protein encoded by the fission yeast cut7+ gene. Nature 347, 563–566.

Harrison BD, Hashemi J, Bibi M, Pulver R, Bavli D, Nahmias Y, Wellington M, Sapiro G, Berman J (2014). A tetraploid intermediate precedes aneuploid formation in yeasts exposed to fluconazole. PLoS Biol 12, e1001815.

Hildebrandt ER, Hoyt MA (2000). Mitotic motors in Saccharomyces cerevisiae. Biochim Biophys Acta 1496, 99–116.

Hill TL, Chen Y (1984). Phase changes at the end of a microtubule with a GTP cap. Proc Natl Acad Sci USA 81, 5772–5776.

Hoyt MA, He L, Loo KK, Saunders WS (1992). Two Saccharomyces cerevisiae kinesin-related gene products required for mitotic spindle assembly. J Cell Biol 118, 109–120.

Inoué S, Salmon ED (1995). Force generation by microtubule assembly/disassembly in mitosis and related movements. Mol Biol Cell 6, 1619–1640.

Jiang K, Toedt G, Montenegro Gouveia S, Davey NE, Hua S, van der Vaart B, Grigoriev I, Larsen J, Pedersen LB, Bezstarosti K, *et al.* (2012). A proteome-wide screen for mammalian SxIP motif-containing microtubule plus-end tracking proteins. Curr Biol 22, 1800–1807.

Joglekar AP, Bouck D, Finley K, Liu X, Wan Y, Berman J, Bloom KS (2008). Molecular architecture of the kinetochore-microtubule attachment site is conserved between point and regional centromeres. J Cell Biol 181, 587–594.

Joglekar AP, Bouck DC, Molk JN, Bloom KS, Salmon ED (2006). Molecular architecture of a kinetochore–microtubule attachment site. Nat Cell Biol 8, 581–585.

Kapitein LC, Peterman EJG, Kwok BH, Kim JH, Kapoor TM, Schmidt CF (2005). The bipolar mitotic kinesin Eg5 moves on both microtubules that it crosslinks. Nature 435, 114–118.

Kashlna AS, Baskin RJ, Cole DG, Wedaman KP, Saxton WM, Scholey JM (1996). A bipolar kinesin. Nature 379, 270–272.
Kops GJPL, Saurin AT, Meraldi P (2010). Finding the middle ground: how kinetochores power chromosome congression. Cell Mol Life Sci 67, 2145–2161.
Kremer JR, Mastronarde DN, McIntosh JR (1996). Computer visualization of three-dimensional image data using IMOD. J Struct Biol 116, 71–76.
Maddox PS, Bloom KS, Salmon ED (2000). The polarity and dynamics of microtubule assembly in the budding yeast Saccharomyces cerevisiae. Nat Cell Biol 2, 36.
Makhnevych T, Houry WA (2013). The control of spindle length by Hsp70 and Hsp110 molecular chaperones. FEBS Lett 587, 1067–1072.
Mitchison T, Wühr M, Nguyen P, Ishihara K, Groen A, Field CM (2012). Growth, interaction, and positioning of microtubule asters in extremely large vertebrate embryo cells. Cytoskeleton (Hoboken) 69, 738–750.
O'Toole ET, Winey M, McIntosh JR (1999). High-voltage electron tomography of spindle pole bodies and early mitotic spindles in the yeast Saccharomyces cerevisiae. Mol Biol Cell 10, 2017–2031.
O'Toole ET, Winey M, McIntosh JR, Mastronarde DN (2002). Electron tomography of yeast cells. Methods Enzymol 351, 81–95.
Pearson CG, Gardner MK, Paliulis LV, Salmon ED, Odde DJ, Bloom K (2006). Measuring nanometer scale gradients in spindle microtubule dynamics using model convolution microscopy. Mol Biol Cell 17, 4069–4079.
Reedy JL, Filler SG, Heitman J (2010). Elucidating the Candida albicans calcineurin signaling cascade controlling stress response and virulence. Fungal Genet Biol 47, 107–116.
Roof DM, Meluh PB, Rose MD (1992). Kinesin-related proteins required for assembly of the mitotic spindle. J Cell Biol 118, 95–108.
Saunders W, Lengyel V, Hoyt M a (1997). Mitotic spindle function in Saccharomyces cerevisiae requires a balance between different types of kinesin-related motors. Mol Biol Cell 8, 1025–1033.
Selmecki A, Forche A, Berman J (2006). Aneuploidy and isochromosome formation in drug-resistant Candida albicans. Science 313, 367–370.
Selmecki A, Forche A, Berman J (2010). Genomic plasticity of the human fungal pathogen Candida albicans. Eukaryotic Cell 9, 991–1008.
Shimogawa MM, Graczyk B, Gardner MK, Francis SE, White EA, Ess M, Davis TN (2006). Mps1 phosphorylation of Dam1 couples kinetochores to microtubule plus ends at metaphase. Curr Biol 16, 1489–1501.
Sprague BL, Pearson CG, Maddox PS, Bloom KS, Salmon ED, Odde DJ (2003). Mechanisms of microtubule-based kinetochore positioning in the yeast metaphase spindle. Biophys J 84, 3529–3546.
Straight AF, Sedat JW, Murray AW (1998). Time-lapse microscopy reveals unique roles for kinesins during anaphase in budding yeast. J Cell Biol 143, 687–694.
Stumpff J, Cooper J, Domnitz S, Moore A, Rankin K, Wagenbach M, Wordeman L (2007). In vitro and in vivo analysis of microtubule-destabilizing kinesins. Methods Mol Biol 392, 37–49.
Tytell JD, Sorger PK (2006). Analysis of kinesin motor function at budding yeast kinetochores. J Cell Biol 172, 861–874.
Varga V, Helenius J, Tanaka K, Hyman AA, Tanaka TU, Howard J (2006). Yeast kinesin-8 depolymerizes microtubules in a length-dependent manner. Nat Cell Biol 8, 957–962.
Westhorpe FG, Straight AF (2013). Functions of the centromere and kinetochore in chromosome segregation. Curr Opin Cell Biol 25, 334–340.
Wilson RB, Davis D, Mitchell AP (1999). Rapid hypothesis testing with candida albicans through gene disruption with short homology regions. J Bacteriol 181, 1868–1874.
Winey M, Mamay CL, O'Toole ET, Mastronarde DN, Giddings TH, McDonald KL, McIntosh JR (1995). Three-dimensional ultrastructural analysis of the Saccharomyces cerevisiae mitotic spindle. J Cell Biol 129, 1601–1615.
Winey M, O'Toole ET (2001). The spindle cycle in budding yeast. Nat Cell Biol 3, E23–E27.
Yeh E, Skibbens R V, Cheng JW, Salmon ED, Bloom K (1995). Spindle dynamics and cell cycle regulation of dynein in the budding yeast, Saccharomyces cerevisiae. J Cell Biol 130, 687–700.